Article

Experimental Investigation of Removal of SO₃ from Flue Gas with Modified Fly Ash Adsorbents

Guiling Xu,* Feihan Chen, Yangjie Qian, Ping Lu, Miaomin Hong, Qi Zhang, and Qiang Zhou

Read Online

ACCESS | Metrics & More | Article Recommendations

ABSTRACT: The removal of nonconventional pollutants in coal-fired power plants, such as SO₃, has been receiving more and more attention. However, due to its unique nature, it is difficult to remove SO₃ effectively with the widely used wet flue gas desulfurization systems. Nowadays, dry-sorbent injection technology has become a promising method for SO₃ emission control in coal-fired power plants. The removal characteristics of SO₃ from flue gas with modified fly ash adsorbents were investigated in a fixed-bed reactor. Factors affecting the adsorption efficiency of SO₃ were studied, including modification method, modified fly ash adsorbent particle size, reaction temperature, and flue gas component. Combined with adsorbent characterization analysis, the adsorption kinetics of SO₃ by modified fly ash adsorbents were carried out with four different adsorption kinetics models. The results show that the SO₃ adsorption efficiency of the fly ash samples increases after modification; the best SO₃ removal performance of fly ash was achieved when 1.5 mol/L NaOH solution was used, with the highest SO₃ adsorption efficiency of up to 98.3%. The modified fly ash adsorbent particle size, water vapor content, and the addition of NO have little effect on the adsorption efficiency of SO₃. As the reaction temperature increases from 250 to 450 °C, the SO₃ adsorption efficiency first increases and then decreases, with an optimal reaction temperature of 350 °C. The addition of SO₂ would compete with SO₃ for adsorption and inhibit the uptake of SO₃ by the adsorbent. Adsorption kinetics data show that external mass transfer and chemical adsorption are the main critical mechanisms affecting the adsorption efficiency of the modified fly ash adsorbent in the SO₃ removal process compared to internal diffusion.
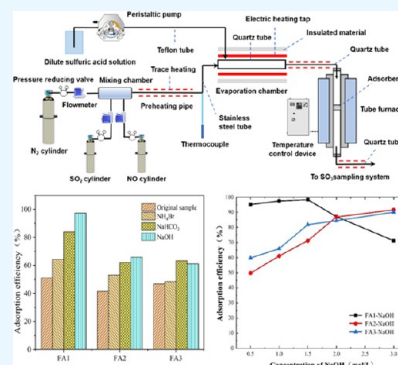
1. INTRODUCTION

With the implementation of increasingly strict environmental standards, ultraclean emission in coal-fired power plants has been extensively advocated and gradually realized.[1,2] In the past several years, studies related to mainstream pollutant emission from coal-fired power plants were mainly focused on nitrogen oxides (NO$_x$), sulfur dioxide (SO$_2$), particulate matter, Hg, etc.[3] Nowadays, controlling nonconventional pollutant sulfur trioxide (SO$_3$), which is in trace amount in the flue gas has been receiving more and more attention.[4−6] With the combustion of high-sulfur coal and the application of oxy-fuel combustion for CO$_2$ capture and storage in power plants, the formation of SO$_3$ is enhanced.[4,7] Although the amount of SO$_3$ in flue gas is far less than that of SO$_2$, its toxicity is ten times that of SO$_2$. SO$_3$ is highly reactive and it can easily react with ammonia (NH$_3$) in a selective catalytic reduction (SCR) reactor to produce sticky ammonium bisulfate (NH$_4$HSO$_4$), causing SCR catalyst deactivation, downstream air preheater plugging.[8] In coal-fired power plant systems, when the flue gas temperature decreases below the acid dew point, sulfuric acid vapor generated by SO$_3$ would condense on the metal surfaces and lead to low-temperature corrosion.[9] Furthermore, when SO$_3$ is released through the stack as submicron acid aerosol, it would cause visible blue plumes. SO$_3$ is also harmful to the atmospheric environment and human health.[10] Therefore, it is urgent to control the emission of SO$_3$ and develop high-efficiency SO$_3$ removal technologies.

Due to its unique nature, SO$_3$ is difficult to remove effectively in widely used wet flue gas desulfurization (WFGD) systems.[11,12] Recently, dry-sorbent injection technology has become a promising method for SO$_3$ emission control.[13,14] The sorbent could be injected before the air preheater, at the economizer outlet or the SCR outlet, and then all SO$_3$ formed in the boiler furnace and SCR can be reduced.[14] The SO$_3$ removal characteristics is mainly influenced by sorbent properties, flue gas parameters, reactor structure parameters, etc.[15,16] Different sorbents have been studied to absorb SO$_3$ in the literature, which are mainly sodium-, calcium-, and magnesium-based substance, such as NaHCO$_3$,[17] Na$_2$CO$_3$,[15]
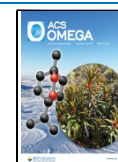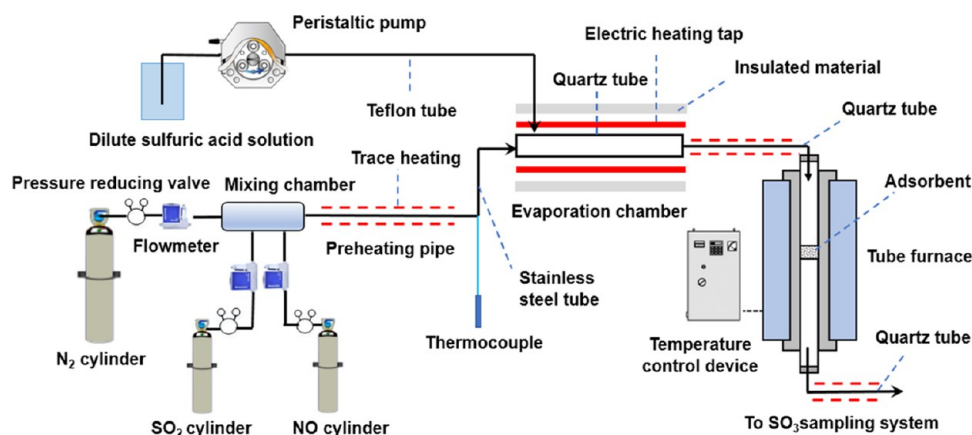
Figure 1. Schematic diagram of SO_3 removal experimental system

Na_2SO_3,[18] $Ca(OH)_2$,[2,13−15,17,19,20] $CaCO_3$,[19] and Mg-$(OH)_2$.[15,17] Meanwhile, some researches focused on metal oxides,[21−23] like CaO, MgO, Na_2O, and K_2O, which are fly ash components, especially CaO,[4,19,22,24] which is one of the main components of fly ash. For the wide industrial applications of dry-sorbent injection technology, selecting a suitable adsorbent material is of great importance.[25] The calcium-based adsorbents have the disadvantage of a low utilization rate, and the sodium- and magnesium-based adsorbents are relatively expensive, leading to high cost.[19,23] Therefore, it is critical to choose high-efficiency and low-cost adsorbents for this SO_3 emission control technique.

Fly ash is the main by-product of the coal combustion process in coal-fired power plants, is predominantly composed of SiO_2, Al_2O_3, and Fe_2O_3 at weight percentages of 50−60, 20−30, and 5−15% respectively, and alkali and alkaline metal oxides, CaO, MgO, Na_2O, and K_2O at weight percentages of 1−40, 0−10, 0−6, and 0−4%, respectively.[23] With increasing coal-fired power generation, a million of tonnes of fly ash could be produced each year, its utilization ratio is less than 30% and the environmentally friendly resource utilization of fly ash is also an attractive method for waste management in coal-fired power plants.[26] Fly ash could be used as low-cost adsorbents for removing various gaseous pollutants in flue gas, such as NO_x, SO_x, Hg, and CO_2, due to its chemical and physical properties.[27,28] Spörl et al.[29] found that higher ash contents are beneficial for capturing SO_3 in a baghouse filter system. Romero et al.[30] reported that depletion of SO_3 concentration in coal-fired boilers was because that part of the generated SO_3 in the boiler had reacted with the alkali oxides in suspended fly ash. Many studies indicated that fly ash could capture acid gaseous sulfur oxides by both adsorption and reaction in a wide temperature range from 30 to 600 °C.[26,31] Developing a novel modified fly ash sorbent for SO_3 removal in the flue gas with high removal capability and low production cost has become a promising topic.[32,33]

The reaction rates of heterogeneous reactions between fly ash and SO_3 are dependent on the chemical and physical characteristics of fly ash particle surface, and the surface characteristics could be modified by the reaction or by adding other chemical species.[34] However, there are rather rare literature reports relating to the modification of fly ash for SO_3 adsorption. Wang et al.[35] studied the adsorption characteristics of ammonium bromide-modified fly ash to SO_3. Some researchers found that alkali modification and alkali activation on fly ash could improve the adsorption capacity of fly ash.[36]

Dindi et al.[37] developed a NaOH-activated fly ash material to investigate the CO_2 capture performance. Gao et al.[38] used novel low-cost NaOH-modified fly ash to prepare dye adsorbent, and analyzed its adsorption mechanism with adsorption kinetics. Tian et al.[39] used the mixture of NaOH and $NaHCO_3$ to modify fly ash to treat the adsorption property of oil-bearing wastewater, and when the optimum volume ratio is 3:1 and the modification temperature is 600 °C, the treatment effect of oily wastewater is the best, reaching 82%. Apart from adsorbent properties, other critical factors that significantly affect SO_3 removal of fly ash are reaction temperature and flue gas component. Meanwhile, the effects of reaction temperature and flue gas component on SO_3 removal characteristics by modified fly ash adsorbents have not been systematically investigated, meanwhile, minimal work has been conducted to reveal the adsorption mechanism of fly ash-based adsorbents for SO_3 removal.

This state of art strategy has motivated this study. In this paper, the removal characteristics of SO_3 from flue gas with modified fly ash adsorbents were investigated on a fixed-bed reactor. Three modified fly ash adsorbents (FA-NH_4Br, FA-$NaHCO_3$, and FA-NaOH) were prepared and characterized. The effects of the modification method, modified fly ash adsorbent particle size, reaction temperature, and flue gas component (SO_3, water vapor, NO, and SO_2) on the adsorption efficiency of SO_3 were discussed. Meanwhile, combined with adsorbent characterization analysis, the adsorption kinetics of SO_3 by the modified fly ash adsorbent was determined with different adsorption kinetics models in order to explore the underlying adsorption removal mechanism of SO_3 by the modified fly ash adsorbent. This work would be helpful for providing a certain reference for further research on the efficient removal of SO_3 from flue gas with low-cost fly ash-based adsorbents and achieving the goal of fly ash resource utilization for pollutant control in coal-fired power plants.

2. EXPERIMENTAL SECTION

2.1. Experimental System. The SO_3 removal experiments were carried out with a fixed-bed reactor apparatus, as shown in Figure 1, which included the SO_3 generation system, the adsorption system, and the SO_3 sampling system. The SO_3 generation system was composed of a peristaltic pump, evaporation chamber, nitrogen (N_2) preheating pipe, etc. A dilute sulfuric acid solution was injected into the high-temperature zone (400 °C) of the evaporation chamber

through the peristaltic pump to generate SO_3. The adsorption system mainly included a heat tracing belt, a vertical tubular furnace, and a quartz tube reactor. The reactor was a quartz tube (10 mm i.d.) with thermocouples placed at the external wall to control the temperature. During each test, the adsorbent sample with a mass of 0.2 g was packed into the adsorption reactor. The generated simulated flue gas entered the reactor from the upper part of the fixed bed and fully reacted with the adsorbent. The connecting tube was heated to above 260 °C and covered with the heat insulation material to prevent SO_3 from condensation. The space velocity is 4780 h^{-1}. The experimental parameters are listed in Table 1.

Table 1. Experimental Parameters

parameters	values	unit
reaction temperature	250, 300, 350, 400, 450	°C
SO_3 concentration	10, 20, 50, 100	$\mu L/L$
water vapor content	6, 8, 10, 12	%
NO concentration	0, 100	$\mu L/L$
SO_2 concentration	0, 1000, 2000	$\mu L/L$

The SO_3 sampling system was built based on the controlled condensation method according to EPA method 8A, as shown in Figure 2. The inner diameter of the spiral condensing tube was 3 mm, and its total length was 2 m. The water bath temperature was 70 °C, and the sampling gas flow rate was 1 L/min. The flue gas leaving the spiral condensing tube passed through four Greenburg–Smith impingers in the ice bath. The first two impingers were filled with 100 mL of 3% hydrogen peroxide solution for the capture of SO_2. The third impinger was filled with 100 mL of deionized water. The last impinger was filled with silica gel to absorb the residual moisture before the flue gas entered the dry gas meter. After the sampling procedure, the spiral condensing tube was rinsed repeatedly with deionized water, and the solution in the impingers was collected. The amount of SO_4^{2-} in the solution was analyzed with an ion chromatograph analyzer (ICS-900, DIONEX). Then, the concentration of SO_3/H_2SO_4 in flue gas could be obtained.

The capacity of the adsorbent for removing SO_3 is measured and the adsorption efficiency η can be calculated as follows

$$\eta = \frac{C_{inlet} - C_{outlet}}{C_{inlet}} \times 100\% \qquad (1)$$

where C_{inlet} is the SO_3 concentration at the inlet and C_{outlet} is the SO_3 concentration at the outlet with units of mmol.

2.2. Materials and Methods. Raw fly ash samples were collected from the electrostatic precipitators of three different pulverized coal power plants in Inter Mongolia, Anhui, and Shanxi in China, which were named FA1, FA2, and FA3, respectively. The mean particle sizes of FA1, FA2, and FA3 are 14.5, 74.1, and 27.9 μm, respectively. The particle size distribution for raw fly ash samples is shown in Figure 3. The main compositions of fly ash samples are listed in Table 2. NH_4Br, $NaHCO_3$, and NaOH were used as the modification agents for fly ash. The modified fly ash adsorbents were prepared by chemical impregnation by referring to the research of Wang et al.[35] Raw fly ash samples with a mass of 10 g were impregnated into 10 ml of NH_4Br, $NaHCO_3$, and NaOH solutions with modification reagent molar concentration of n mol/L at room temperature, respectively. Here, n can be varied to investigate the effect of the molar concentration of the modification reagent on the SO_3 removal characteristics of modified fly ash. The solutions were stirred at 800 rpm with a magnetic stirrer for 2 h, and then were placed in a fume hood for 12 h. After pouring out the supernatant liquid, the samples were dried in a thermostatic drying oven at 105 °C for 24 h. The dried samples were ground and sieved with standard sieves into different particle sizes. The modified fly ash adsorbents were labeled according to the modification reagent type and its molar concentration. For instance, when FA1 was modified with 1.5 mol/L NaOH solution, the modified fly ash was labeled as FA1-1.5 NaOH.

The specific surface area and pore structure parameters of modified fly ash adsorbents were measured using a specific surface area and porosity analyzer (NOVA1000e, Quanta chrome). The apparent morphology and microstructure of adsorbent samples were tested by high-resolution scanning electron microscopy (JSM-5610 LV, JEOL, Japan). The particle size and particle size distribution of adsorbent samples were measured using a laser particle size analyzer (ST-1076, Yishite Instrument Ltd., China). In order to further study the mechanism of SO_3 removal by modified fly ash adsorbent, an X-ray powder diffractometer (D/max 2500/PC, Nippon
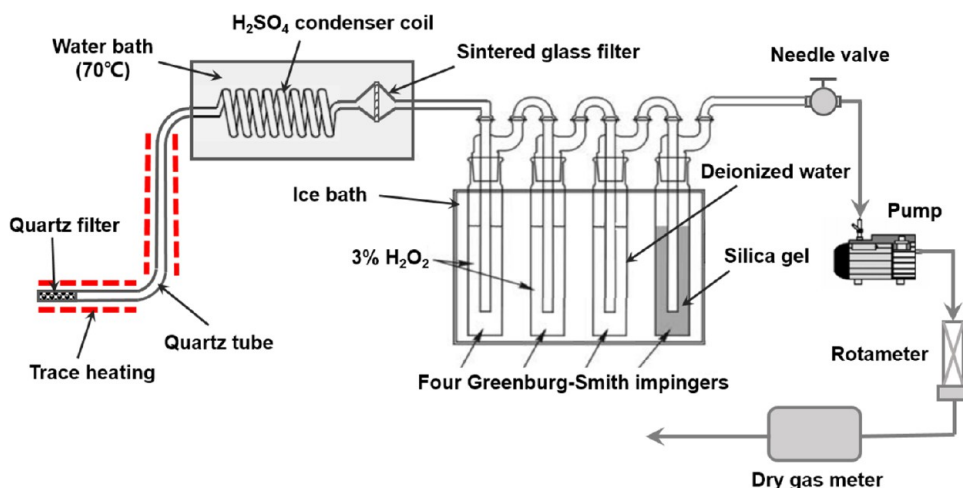
Figure 2. Schematic diagram of the SO_3 sampling system.

(a) FA1

(b) FA2

(c) FA3
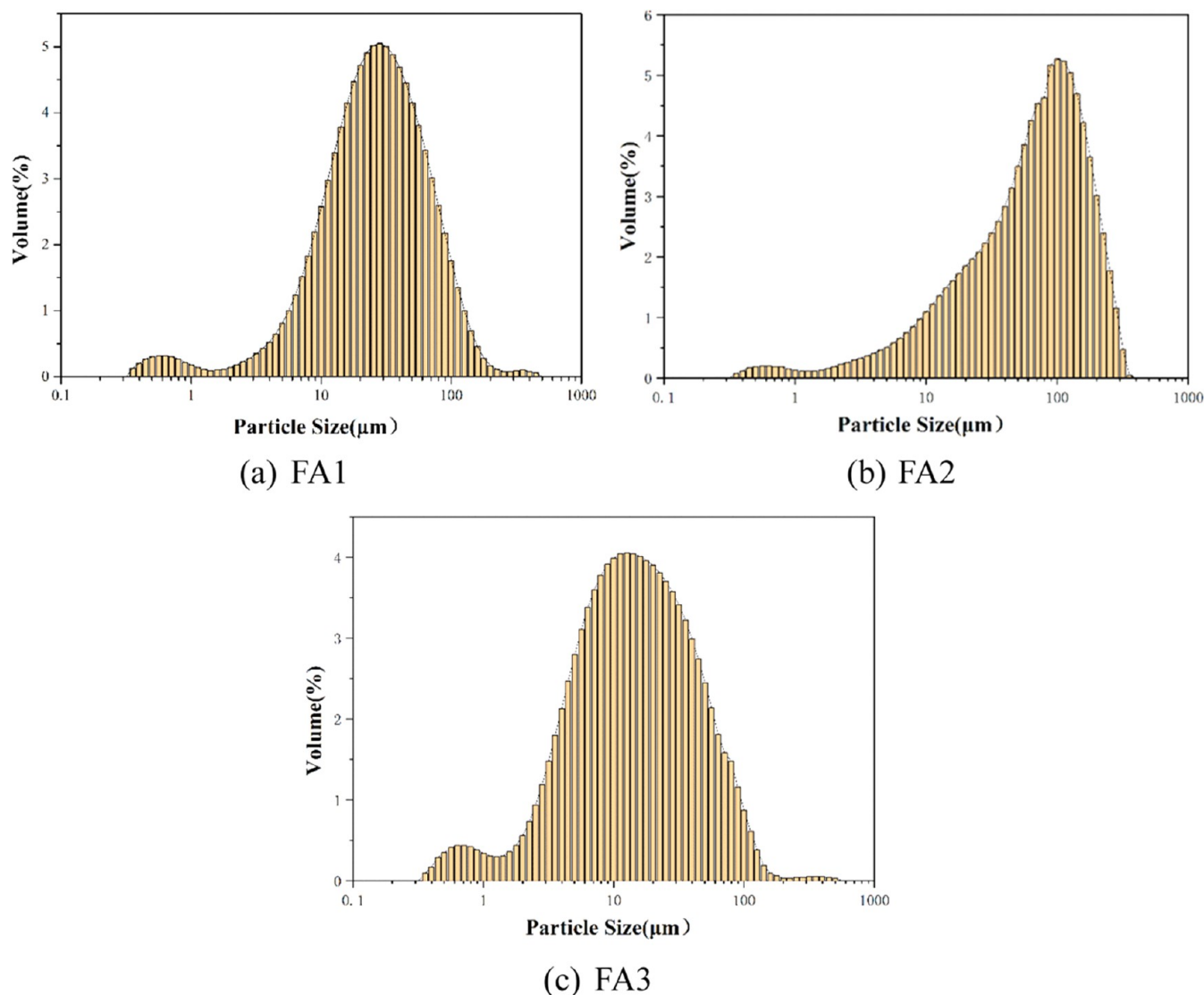
Figure 3. Particle size distribution for raw fly ash samples.

Table 2. Main Compositions of Fly Ash Samples

sample	content (%)				
	SiO_2	Al_2O_3	Fe_2O_3	CaO	K_2O
FA1	32.929	14.464	16.794	24.148	3.038
FA2	51.36	30.34	8.461	3.033	1.909
FA3	41.916	28.327	12.749	9.013	2.428

Science Company, Japan) was used to determine the crystallinity contained in the sample. The transformation of the functional group was measured using a Fourier Transform Infrared Spectrometer (Vertex 70, Bruker, Germany), and the chemical composition was detected using an X-ray Fluorescence Spectrometer (AXIOS-MAX, PANalytical B.V., Netherlands).

3. RESULTS AND DISCUSSION

3.1. Effect of the Modification Method on SO_3 Adsorption Efficiency. *3.1.1. Effect of the Modification Solution Type.* Figure 4 shows the effect of the modification solution type on SO_3 adsorption efficiency. SO_3 adsorption efficiency of the modified fly ash samples increases after
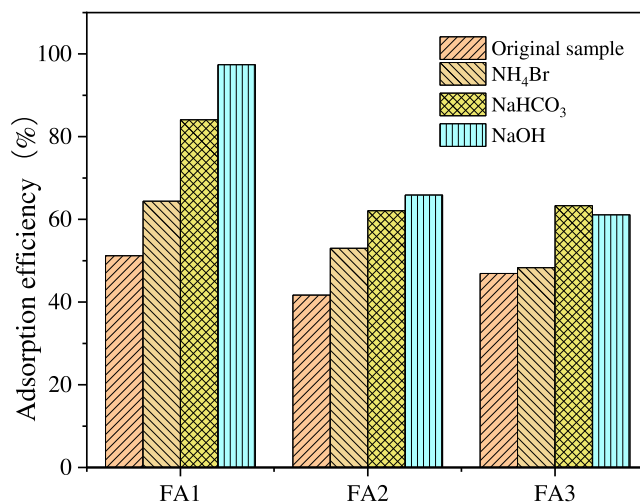
Figure 4. Effect of modification of the solution type on SO_3 adsorption efficiency.

modification. Meanwhile, the fly ash samples modified with NaOH basically show the greatest adsorption ability of SO_3,

WD=7.1mm Mag=10.00KX Width=11.43μm

(a)   FA1

WD=6.8mm Mag=10.00KX Width=11.43μm

(b)   FA1-NaOH

WD=7.0mm Mag=5.00KX Width=22.87μm

(c)   FA2

WD=7.0mm Mag=5.00KX Width=22.87μm

(d)   FA2-NaOH

WD=7.0mm Mag=5.00KX Width=22.87μm

(e)   FA3

WD=7.1mm Mag=5.00KX Width=22.87μm

(f)   FA3-NaOH
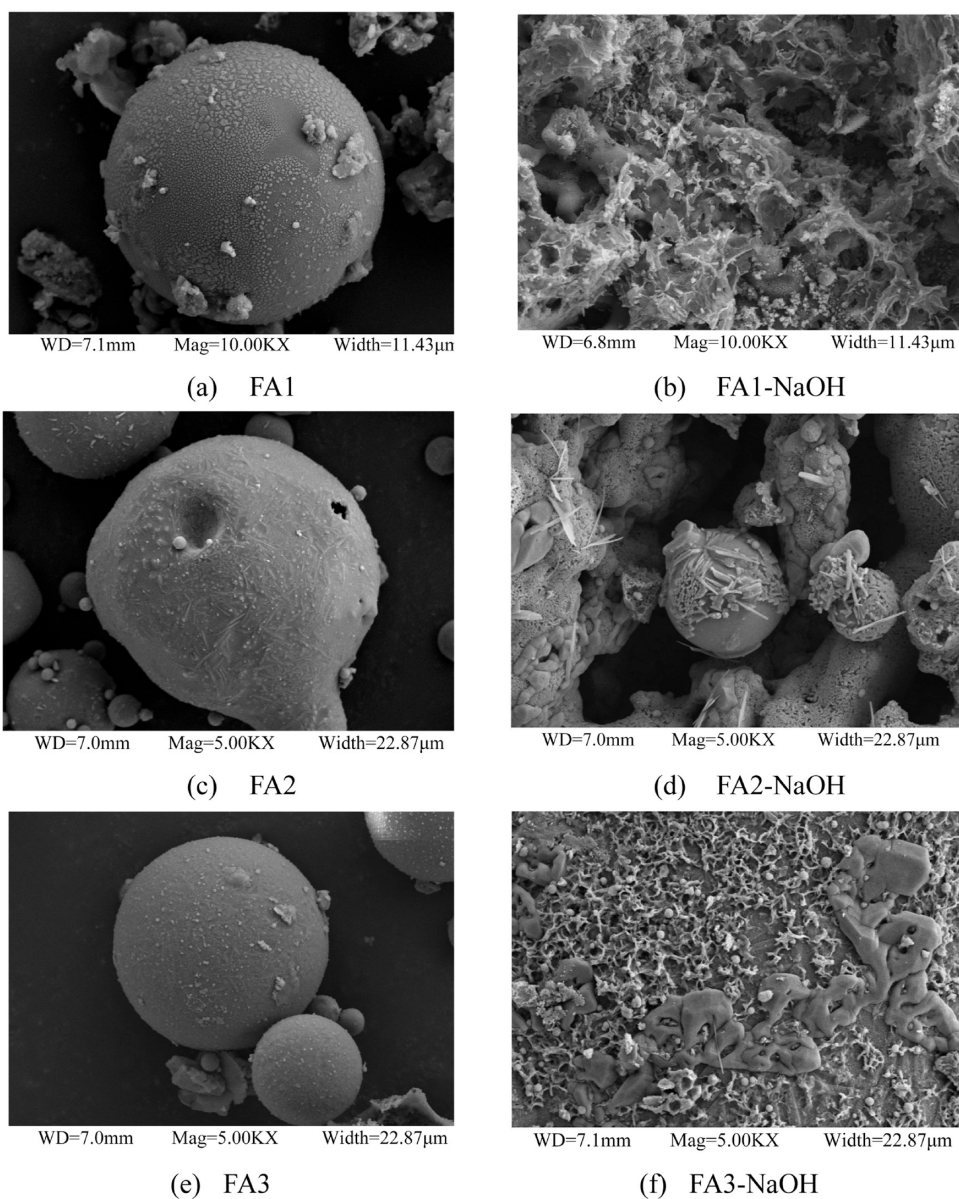
Figure 5. SEM photos of fly ash samples before and after modification.

(a) SO_3 adsorption capacity

(b) SO_3 adsorption efficiency
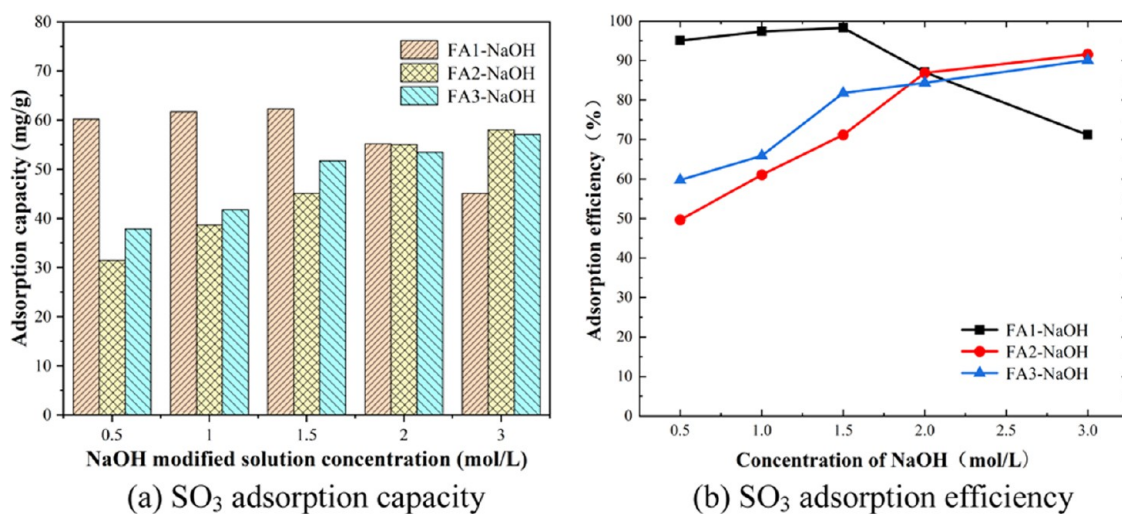
Figure 6. Effect of the NaOH-modified solution concentration.

while fly ash samples modified with NH_4Br have the poorest SO_3 adsorption ability. NaOH has the strongest alkalinity among the three modification solutions. After being modified, the vitreous structure in fly ash particles could be destroyed and the internal metal oxides are released and become active.[32] The most stable form of SO_3 binding with these oxides was the combination of the S atom of SO_3 and O of oxide to form stable sulfate.[23] The porosity, pore volume, and specific surface area of the fly ash particles increase, improving the physical adsorption ability, and the functional group on the particle surface changes, enhancing the chemical adsorption ability.[40] $NaHCO_3$ solution is weakly alkaline, its enhancement effect is not as obvious as that of NaOH. The fly ash modified with NH_4Br would decompose gaseous NH_3 at high temperatures, which can react with SO_3 and H_2O in the flue gas. However, the promoting effect on SO_3 adsorption is not so good.

Figure 5 compares the SEM micrographs of fly ash samples before and after modification. As shown in Figure 5a,c,e, the raw fly ash samples are mainly in granular morphology, smooth spherical particles are dominant, with fine porous material adhering to the particle surface. As shown in Figure 5b,d,f, the particle surface is loosened, the porosity of the structure increases, and the specific surface area increases correspondingly. During the modification process, activation of raw fly ash begins with the digestion of vitreous-phase silica and alumina by the effect of modification solutions. The physical and chemical adsorption ability of fly ash particles can both be improved after being modified.[41,42]

3.1.2. Effect of NaOH Modification Solution Concentration. Figure 6 shows the effects of NaOH modification solution concentration on the SO_3 adsorption capacity and efficiency, respectively. As for FA1, when NaOH modification solution concentration increases from 0.5 to 3 mol/L, the SO_3 adsorption capacity and efficiency of modified fly ash both first increase and then decrease. When the modification solution concentration is 1.5 mol/L, the SO_3 adsorption efficiency of modified fly ash reaches the maximum value, which is 98.3%, and the SO_3 adsorption capacity is 62.3 mg/g. However, for FA2 and FA3, as NaOH modification solution concentration increases from 0.5 to 3 mol/L, the SO_3 adsorption capacity and efficiency of modified fly ash show an increasing trend. When the NaOH modification solution concentration exceeds 2 mol/ L, the increasing trend for SO_3 adsorption capacity and efficiency tends to flatten. It may be because after being modified with NaOH solution, a desilication reaction will occur in the fly ash particles. The amorphous glass phase and quartz component of fly ash are partially dissolved in NaOH solution, leading to decreasing Si/Al ratio and increasing micropores.[43] With the increase in the NaOH solution concentration, the pore volume and specific surface area of fly ash particles increase, the alkalinity of modified fly ash increases, and the adsorption efficiency of SO_3 increases gradually. However, when the NaOH modification solution exceeds a certain value, e.g., 1.5 mol/L for FA1, the crystal structure inside fly ash particles becomes loose and the internal structure would collapse,[44] leading to the decreasing SO_3 adsorption ability. Then, the SO_3 adsorption capacity and efficiency of modified fly ash will show a variation tendency of decrease.

3.1.3. Characterization Analysis of Modified Fly Ash. *3.1.3.1. SEM Analysis.* Figure 7 shows the SEM micrographs for FA1-1.5 NaOH before and after adsorption. It can be seen from Figure 7a that the adsorbent particle before adsorption

WD=8.8mm   Meg=10.00KX   Width=11.43μm

(a) Before adsorption

WD=4.7mm   Meg=10.00KX   Width=11.43μm
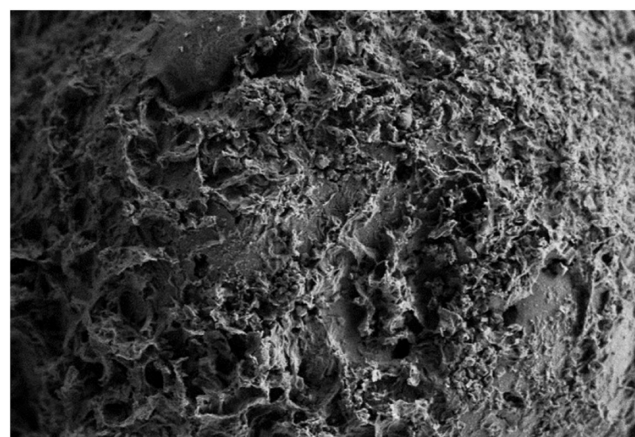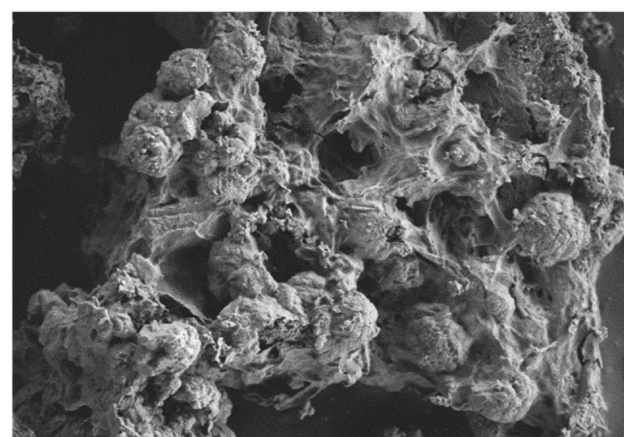
(b) After adsorption

Figure 7. SEM micrographs.

was relatively complete, and the particle surface was rough, which provides a large specific surface area for SO_3 adsorption. After adsorption, as shown in Figure 7b, the overall morphology of the adsorbent particle changed greatly, and a serious adhesion phenomenon occurred on the surface of the particles, which may be caused by the chemical reaction between SO_3 and the surface-active substance of the adsorbent. Meanwhile, the reaction products covered the surface of the adsorbent particles, reducing the specific surface area, and the formed agglomeration substance prevented the internal diffusion of SO_3 in the adsorbent.[45]

3.1.3.2. XRF Analysis. Table 3 lists the changes of the S and Si elemental content before and after SO_3 adsorption by FA1-1.5 NaOH. It can be seen that the Si content increases slightly because the adsorbent was mixed with high-purity quartz sand,

Table 3. Changes of the S and Si Elemental Content before and after SO_3 Adsorption

element	content (%)	
	Si	S
before adsorption	30.276	0.153
after adsorption	31.024	3.452
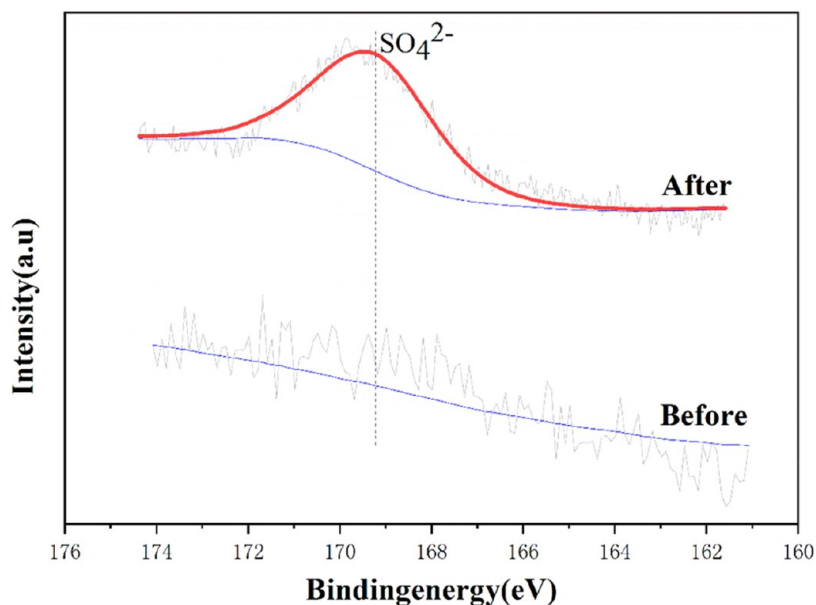
Figure 8. XPS spectra.

and a small part of quartz sand remained in the reacted samples after the experiment.[46] Before adsorption, the content of the S element in the adsorbent was very low, only 0.153%. After adsorption, the content of the S element in the sample increased to 3.452%.

3.1.3.3. XPS Analysis. Figure 8 illustrates the XPS spectra of S element for FA1-1.5 NaOH before and after adsorption. There was no obvious characteristic peak before adsorption, indicating that the modified fly ash adsorbent did not contain the S element before adsorbing SO_3. Furthermore, the peak intensity of the S element changed obviously after the modified fly ash adsorbed SO_3. There was an obvious characteristic peak in the S 2p spectrum after adsorption, which was located near the electron binding energy of 169 eV. The characteristic peak may come from $Al_2(SO_4)_3$, $CaSO_4$, Na_2SO_4, and K_2SO_4.[47,48] It was indicated that there was metal sulfate in the products after adsorption, which was formed by the chemical reaction between SO_3 in flue gas and alkali metal oxides in the modified fly ash adsorbent.

3.1.3.4. FTIR Analysis. Figure 9 presents the Fourier transform infrared (FTIR) spectra of FAl-1.5 NaOH before and after adsorption. There is no obvious change in FTIR spectra of the modified fly ash adsorbent before and after adsorption, indicating that the structure of the modified fly ash adsorbent did not change after adsorption. However, the positions and contents of some functional groups changed. The wide peak at 3200−3550 cm^{-1} is alcohol O−H stretching vibration.[49] After adsorption, the peak intensity is significantly reduced, which may be because the O−H bond was involved in the adsorption process of SO_3 by the modified fly ash adsorbent. Alcohol O−H bending vibration occurs at 1330−1420 and 750−800 cm^{-1}, which may be due to the reaction of water vapor in flue gas during the adsorption process, forming a small amount of O−H bonds on the surface of the adsorbent.[50] 830−1110 cm^{-1} is Si−O stretching vibration, and the characteristic peak shifted after the reaction, indicating that the Si−O bond also plays a certain role in the adsorption of SO_3.[51] It should be noted that at 608−620 cm^{-1} a new characteristic peak appeared after adsorption, which was the sulfate ion absorption peak. As the concentration of SO_3 in flue
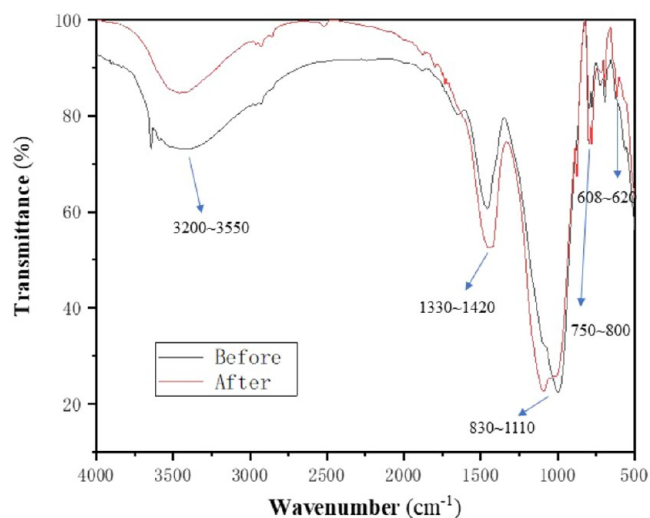
Figure 9. FTIR spectra.

gas is extremely low, resulting in the low intensity of the characteristic peak for sulfate ions. The appearance of sulfate ion shows that the modified fly ash adsorbent has a chemical adsorption effect on SO_3.

3.1.4.5. XRD Analysis. Figure 10 shows the XRD patterns of SO_3 adsorbed by FA1-1.5 NaOH before and after adsorption. After adsorption, the diffraction peak of SiO_2 was enhanced. It was because in the fixed-bed adsorption experiments, the modified fly ash adsorbent and high-purity quartz sand were mixed together and fixed with quartz cotton in the reactor. After the experiments, a small portion of quartz sand and quartz cotton remained in the used adsorbent sample. The new diffraction peaks of $KFe(SO_4)_2(H_2O)_2$, $CaSO_4$, and Na_2SO_4 appeared in the adsorbent after the adsorption reaction, which is due to the chemical reaction among alkali metal oxide in fly ash, sulfur trioxide, and water vapor. At a diffraction angle 2θ of 27°, there was a substance both before and after adsorption, which was Na_2SiO_3. It was due to the chemical reaction
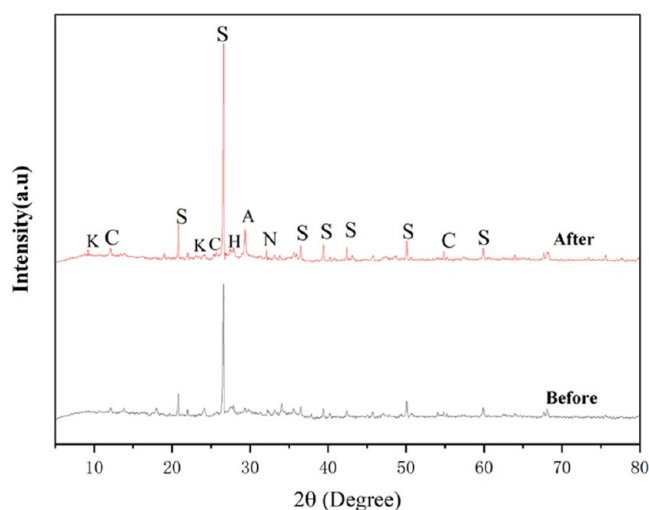
Figure 10. XRD patterns: K:$KFe(SO_4)_2(H_2O)_2$ C:$CaSO_4$ N:Na_2SO_4 A:$Al_2(SO_4)_3 \bullet 8H_2O$ S:SiO_2 H:Na_2SiO_3.

between sodium hydroxide and silica during the modification process that α-phase sodium disilicate was formed.[52]

3.2. Effect of Modified Fly Ash Adsorbent Particle Size on SO$_3$ Adsorption Efficiency. Figure 11 illustrates the effects of modified fly ash adsorbent particle size on SO$_3$ adsorption capacity and efficiency, respectively. When the modified fly ash adsorbent particle size is in the range of 0.065−0.154 mm, the SO$_3$ adsorption capacity varies between 56.5 and 60.5 mg/g, and the SO$_3$ adsorption efficiency is in the range of 91.4−95.5% with the maximum difference of SO$_3$ adsorption of only 4.1%. Within the modified fly ash adsorbent particle size range investigated in this study, modified fly ash adsorbent particle size has little influence on the SO$_3$ adsorption efficiency. The reactions between adsorbent particles and SO$_3$ are composed of two parts, first, the surface reaction between SO$_3$ and particle surface which is not covered by the product layer, and second, the diffusing of SO$_3$ through the product layer and the reaction between SO$_3$ and the

unreacted adsorbent core.[20] Therefore, the absorption of SO$_3$ can be divided into the chemical kinetics-controlled stage and product layer diffusion-controlled stage.[13] The reduction in the particle size cannot achieve obvious improvement in SO$_3$ adsorption efficiency because the diffusion resistance of individual particles is dominant. Thibault et al.[22] reported the results of adsorption of SO$_3$ by CaO and MgO particles, and found that for efficient capture of SO$_3$, small particle size and open macropore structure are both of great importance. Their results showed that the adsorption rates are independent of the particle size in the range of 0.06−0.33 mm. Kocaefe et al.[53] compared the sulfation rates of calcium, magnesium, and zinc oxides with SO$_2$ and SO$_3$, experiments were conducted with various oxide particle sizes (0.071−0.151 mm), and their data indicated that particle size in their experimental range has an insignificant effect on the reaction rates for all the three different kinds of oxide particles. Here, the particle size of modified fly ash was 0.065−0.074 mm in subsequent experiments of this study.

3.3. Effect of the Reaction Temperature on SO$_3$ Adsorption Efficiency. Figure 12 presents the effects of reaction temperature on SO$_3$ adsorption capacity and efficiency, respectively. Considering that the flue gas outlet temperature of the SCR reactor is commonly about 350 °C, 250/300/350/400/450 °C is selected as the reaction temperature. As the reaction temperature increases, the SO$_3$ adsorption capacity and efficiency both first increase and then decrease. The SO$_3$ adsorption of modified fly ash includes physical adsorption and chemical adsorption. Physical adsorption is the adsorption of SO$_3$ on the surface and the pore structure of the adsorbent particles due to the action of van der Waals force. The heat required for the physical adsorption process is very low, so low temperature is favorable for physical adsorption.[54] Chemical adsorption depends on the reaction of active components in the adsorbent particles with SO$_3$ in the flue gas, which involves the breaking and formation of chemical bonds. The changes of chemical bonds require a certain amount of adsorption heat and activation energy. As the reaction temperature increases, the chemical reaction rate
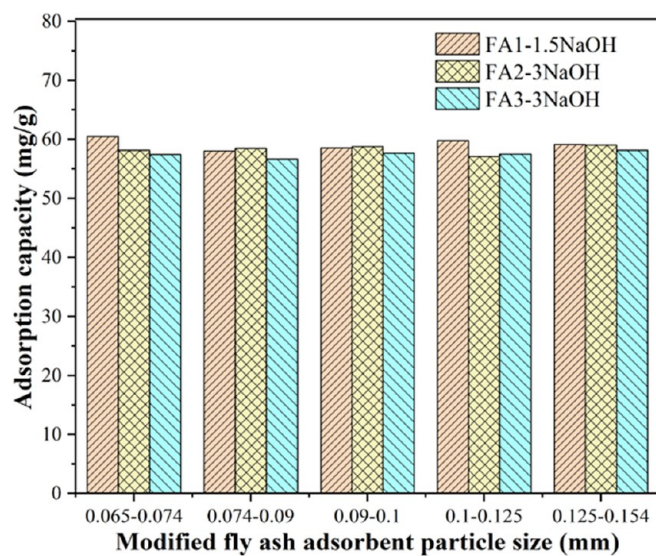
(a) SO$_3$ adsorption capacity
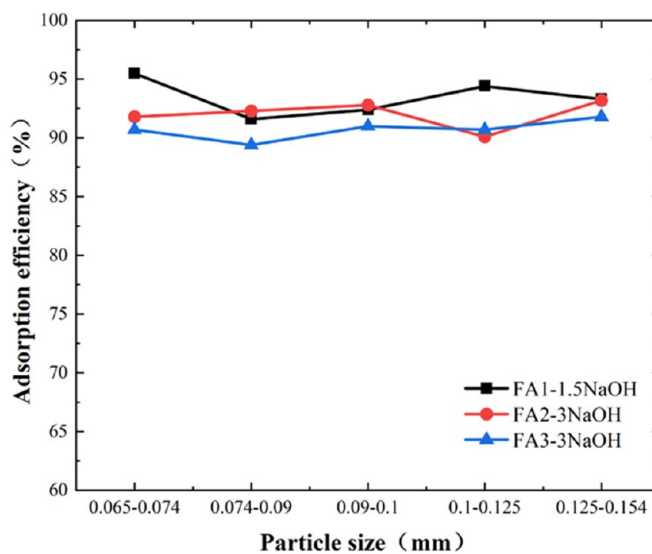
(b) SO$_3$ adsorption efficiency

Figure 11. Effect of the modified fly ash adsorbent particle size.

(a) SO$_3$ adsorption capacity   (b) SO$_3$ adsorption efficiency
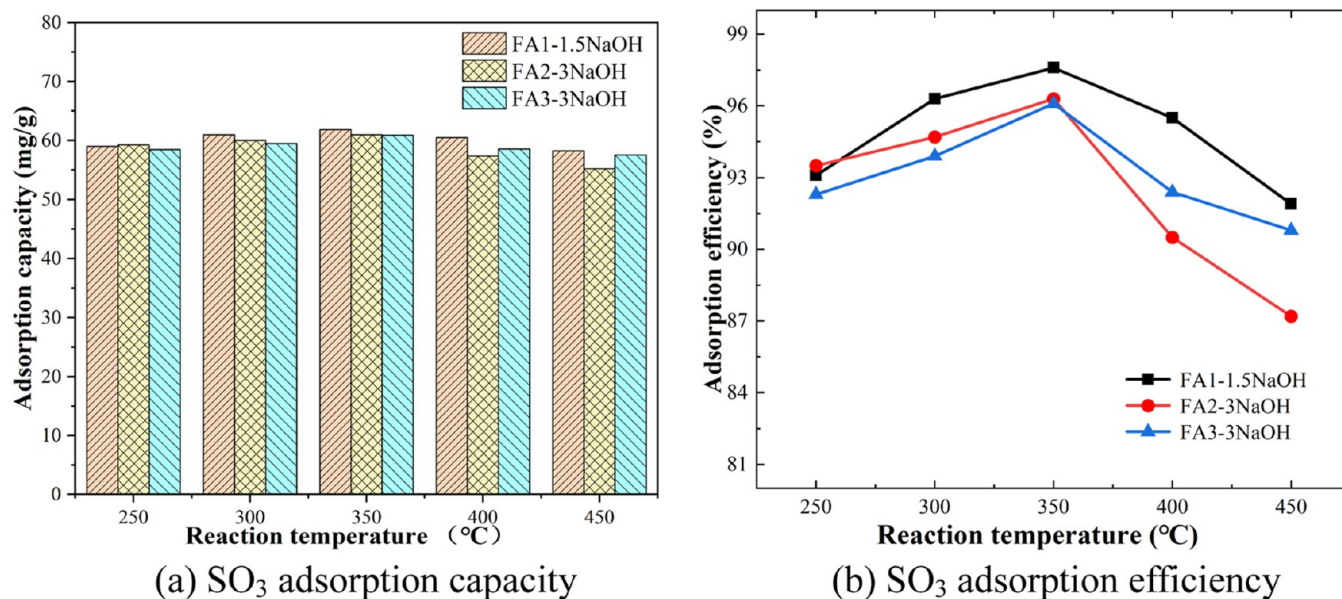
Figure 12. Effect of the reaction temperature.

(a) SO$_3$ adsorption capacity   (b) SO$_3$ adsorption efficiency
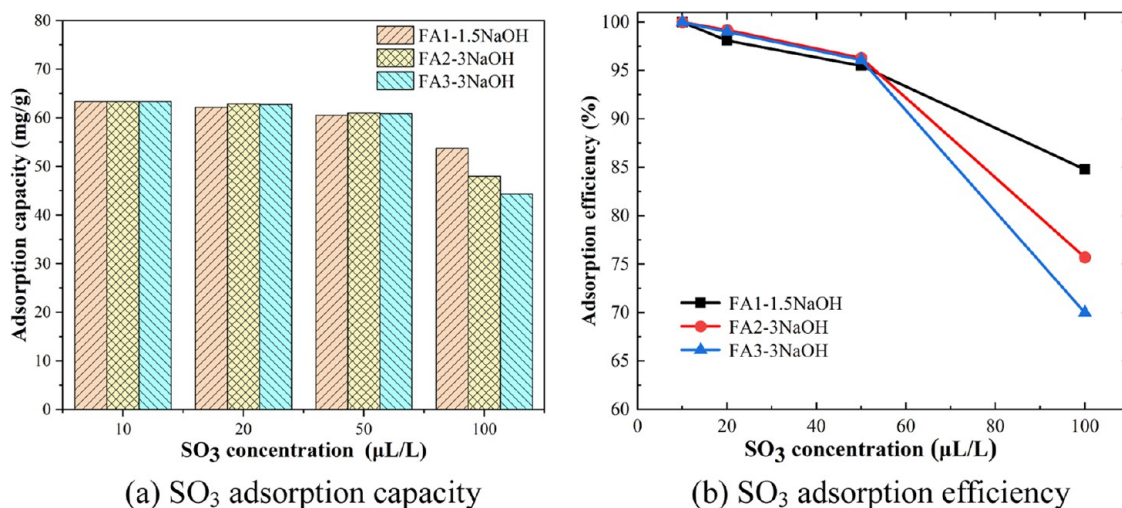
Figure 13. Effect of SO$_3$ concentration.

increases correspondingly, the SO$_3$ adsorption capacity and efficiency both increase. When the reaction temperature increases to 350 °C, the SO$_3$ adsorption capacity and efficiency both reach their maximum values, corresponding to the optimal reaction temperature. With a further increase in the reaction temperature, the active components in the adsorbent particles may be inactivated as the temperature becomes too high, the chemical reaction rate decreases, and the chemical adsorption ability decreases. Meanwhile, the SO$_3$ adsorbed in the modified fly ash particles may be easy to desorb at high reaction temperatures, and the physical adsorption ability decreases. Therefore, when the reaction temperature exceeds 350 °C, the SO$_3$ adsorption capacity and efficiency both show a decreasing tendency. Wang et al.[19] reported SO$_3$ adsorption experimental results with Ca(OH)$_2$, CaO, and CaCO$_3$ under medium temperatures (300, 350, and 400 °C), and results show that as the reaction temperature increases, the final sulfuration rate of the sorbents increases, and the breakthrough curves formed for different alkaline substances are different. Zheng et al.[15] found that the SO$_3$ adsorption efficiency for

Na$_2$CO$_3$ increases as the reaction temperature increases from 150 to 300 °C, while when the reaction temperature is above 300 °C, the temperature has little influence on the SO$_3$ adsorption efficiency. Their results show that the SO$_3$ adsorption efficiency at 350 °C is lower than that at 300 °C, which is because when the reaction temperature exceeds 300 °C, the gas diffusion becomes the controlling step for SO$_3$ adsorption compared to the gas–solid interface reaction.

3.4. Effect of Flue Gas Components on SO$_3$ Adsorption Efficiency. *3.4.1. Effect of the SO$_3$ Concentration.* In order to explore the effect of SO$_3$ concentration on the SO$_3$ adsorption performance of modified fly ash adsorbents, the initial SO$_3$ concentration in flue gas was 10 to 100 μL/L. The particle size of modified fly ash was 0.065–0.074 mm. The reaction temperature was 350 °C, and the water vapor content was 10%. Figure 13 shows the effects of SO$_3$ concentration on SO$_3$ adsorption capacity and efficiency, respectively. As the SO$_3$ concentration increases from 10 to 100 μL/L, the SO$_3$ adsorption capacity and efficiency for three different modified fly ash adsorbents show a variation tendency
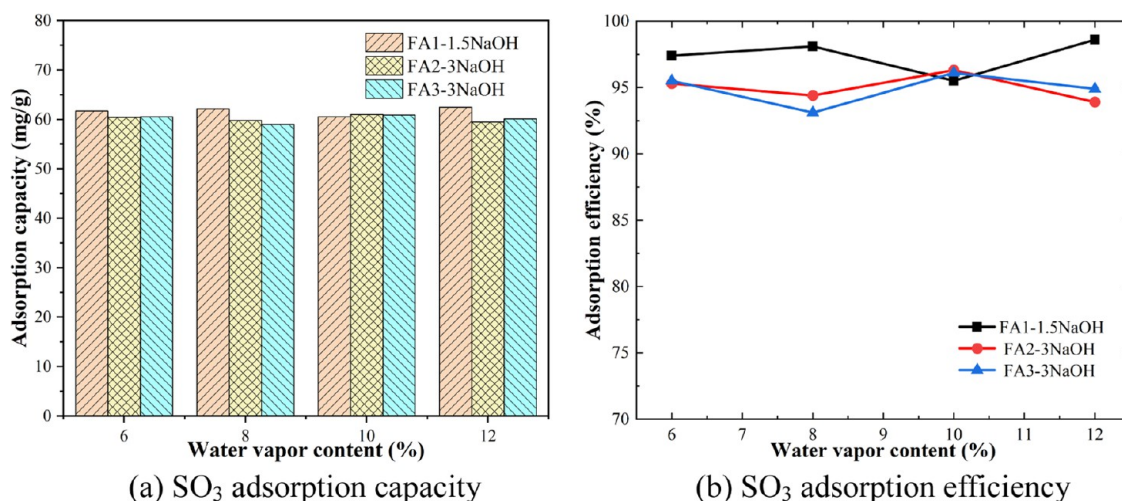
Figure 14. Effect of water vapor content.
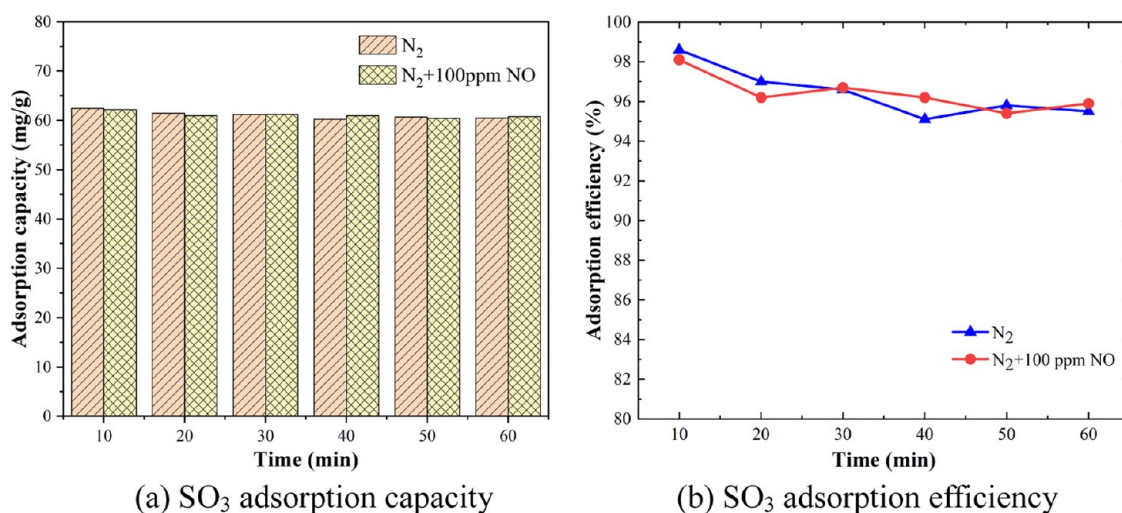
Figure 15. Effect of NO concentration.

of decrease. When the SO_3 concentration is less than 50 $\mu L/L$, the decreasing tendency is not so obvious, while when the SO_3 concentration exceeds 50 $\mu L/L$, the SO_3 adsorption capacity and efficiency for different modified fly ash samples both decrease significantly, except for the FA1 modified with 1.5 mol/L NaOH solution. This may be because with the increase in SO_3 concentration, part of the SO_3 passes through the modified fly ash adsorbent layer directly without reacting with the adsorbent, resulting in decreasing SO_3 adsorption efficiency. Meanwhile, as the active chemical bonds on the surface of the modified fly ash particles continue to react with SO_3, the number of active chemical bonds decreases and the probability of the active adsorption sites of the modified fly ash particles in contact with SO_3 is reduced, leading to a decrease in the SO_3 adsorption efficiency.

3.4.2. Effect of Water Vapor Content. Figure 14 represents the effect of water vapor content on SO_3 adsorption capacity and efficiency, respectively. The SO_3 concentration in the flue gas was 50 $\mu L/L$. The particle size of modified fly ash was 0.065−0.074 mm. The reaction temperature was 350 °C. As the research background of this study is to control the SO_3 emission in the flue gas of coal-fired power plants, and the water vapor content was chosen from 6 to 12% in order to

simulate the real water vapor content of coal flue gas under the actual engineering conditions. As shown in Figure 14, when the water vapor content is in the range of 6−12%, the SO_3 adsorption capacity differences for all three differently modified fly ash adsorbents are small, and the water vapor content has little influence on the SO_3 adsorption efficiency. Zheng et al.[15] carried out SO_3 removal experiments by alkaline sorbents, they used catalytic oxidation of SO_2 to generate SO_3, they compared the results under the condition without water vapor and under the condition of 1% water vapor volume fraction, and found that the presence of water vapor could promote the conversion of SO_3 into H_2SO_4, enhancing the SO_3 adsorption performance. Different from their experiments, the SO_3 in this paper is generated based on the dilute sulfuric acid heating method, water vapor is always present in simulated flue gas. Under the reaction temperature of 350 °C, the amount of water vapor in the flue gas is far more than that needed to form H_2SO_4. According the calculation of flue gas thermodynamic acid dew point,[9] as the water vapor content increases from 6 to 12%, the acid dew point of flue gas increases gradually, but it is lower than the reaction temperature in the adsorption bed in these experiments. After the SO_3 is absorbed by the modified fly ash adsorbents,
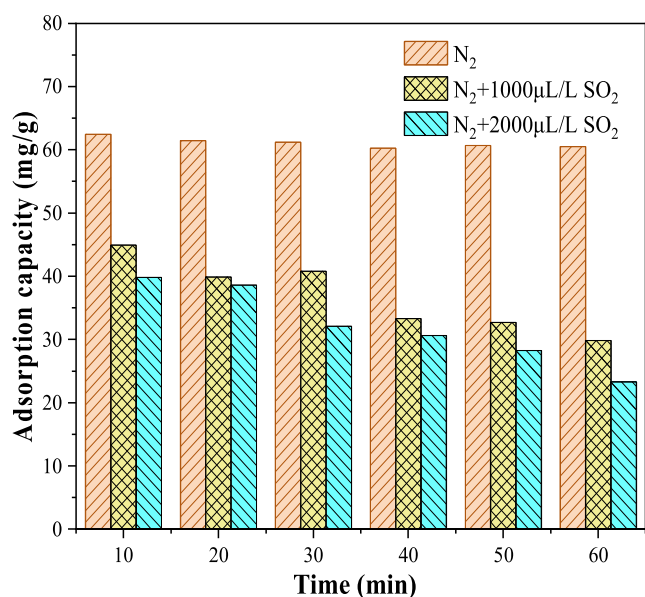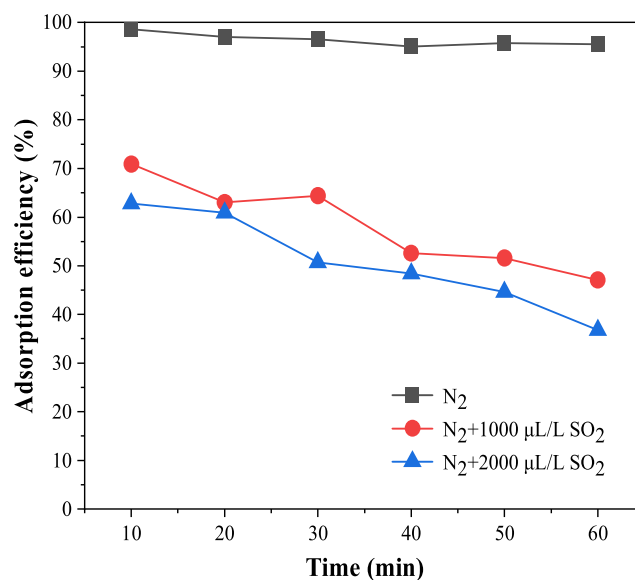
Figure 16. Effect of the SO_2 concentration.

the sulfuric acid vapor entering the air preheater is greatly reduced, which can effectively avoid the corrosion and ash blocking of the air preheater.

3.4.3. Effect of the NO Concentration. Figure 15 represents the effect of NO concentration on SO_3 adsorption capacity and efficiency, respectively. The SO_3 concentration in the flue gas was 50 μL/L. The particle size of modified fly ash was 0.065–0.074 mm. The reaction temperature was 350 °C. The water vapor content was 10%. The modified fly ash adsorbent was FA1-1.5 NaOH. When 100 μL/L NO was added to the flue gas, the SO_3 adsorption capacity and efficiency were not much different from those without NO in the flue gas. In the literature, there is rare research on the effect of NO concentration on SO_3 adsorption performance. Yang et al.[32] carried out simultaneous removal experiments of NO and SO_2 by modified fly ash, and found that the NO concentration variation had little effect on SO_2 removal efficiency. Based on the results of this paper, it can be inferred that the adsorption processes of SO_3 and NO for modified fly ash adsorbents do not affect each other, and there seems to be no competitive adsorption between SO_3 and NO.

3.4.4. Effect of the SO_2 Concentration. Figure 16 represents the effect of SO_2 concentration on SO_3 adsorption capacity and efficiency, respectively. The SO_3 concentration in the flue gas was 50 μL/L. The particle size of modified fly ash was 0.065–.074 mm. The reaction temperature was 350 °C. The water vapor content was 10%. The modified fly ash adsorbent was FA1-1.5 NaOH. As shown in Figure 16, when there is no SO_2 in the flue gas, the SO_3 adsorption capacity is larger than 60 mg/g within 60 min, and the SO_3 adsorption efficiency remains higher than 95%. After 1000 μL/L SO_2 is added to the flue gas, the SO_3 adsorption capacity and efficiency both decrease significantly. Meanwhile, the SO_3 adsorption efficiency decreases gradually with the increasing reaction time. When the SO_2 concentration was further increased to 2000 μL/L, the SO_3 adsorption capacity and efficiency become lower. The increase in SO_2 concentration of the flue gas would inhibit SO_3 adsorption and removal by the

modified fly ash adsorbents. This may be because there exists competitive adsorption between SO_2 and SO_3,[13] and the increasing SO_2 concentration decreases the SO_3 adsorption efficiency of modified fly ash adsorbents.

The concentration of SO_2 in the flue gas is dozens of times that of SO_3, which reduces the probability of SO_3 contact with the active sites, and the SO_3 adsorption capacity for the modified fly ash adsorbents decreases. The number of active sites on the surface of the adsorbent is limited. The reaction between SO_2 and the active sites will lead to irreversible loss of active sites due to the formation of sulfites/sulfates.[10] As the reaction time increases, the active sites decrease concomitantly, and the pore structures are blocked by the substance formed, and the SO_3 adsorption efficiency decreases. He et al.[13] investigated competitive adsorption between SO_3 and SO_2 by calcium hydroxide, and they pointed out that the SO_3 and SO_2 selectivity of the adsorbent influences its SO_3 removal efficiency. The SO_3 and SO_2 adsorption processes can be divided into a chemical kinetics-controlled stage and the product layer diffusion-controlled stage. The SO_3 reactivity is much higher than that of SO_2, the SO_3 molecule is relatively larger than the SO_2 molecule,[20] and the SO_3 concentration in the flue gas is much lower than that of SO_2. In the chemical kinetics-controlled stage, the increasing SO_2 concentration decreases the SO_3 adsorption efficiency because of the competitive consumption of the active sites between SO_2 and SO_3. In the product layer diffusion-controlled stage, the effective diffusion coefficient for SO_3 was lower than that for SO_2, the slower diffusion of SO_3 through the product layer decreases the SO_3 adsorption efficiency. Liu et al.[4] also pointed out that although SO_3 has strong interactions with alkaline adsorbents than SO_2, the increase in the SO_2 concentration could decrease SO_3 adsorption. Some researchers have shown that SO_2 may be oxidized to SO_3 by the metal oxide on the adsorbent, which inhibits the adsorption efficiency of SO_3 by the adsorbent. The consumption of SO_2 on the surface functional group of the adsorbent will reduce the removal of SO_3 by the adsorbent.

(a) Pseudo-first-order model

(b) Pseudo-second-order model

(c) Internal diffusion model

(d) Elovich adsorption model
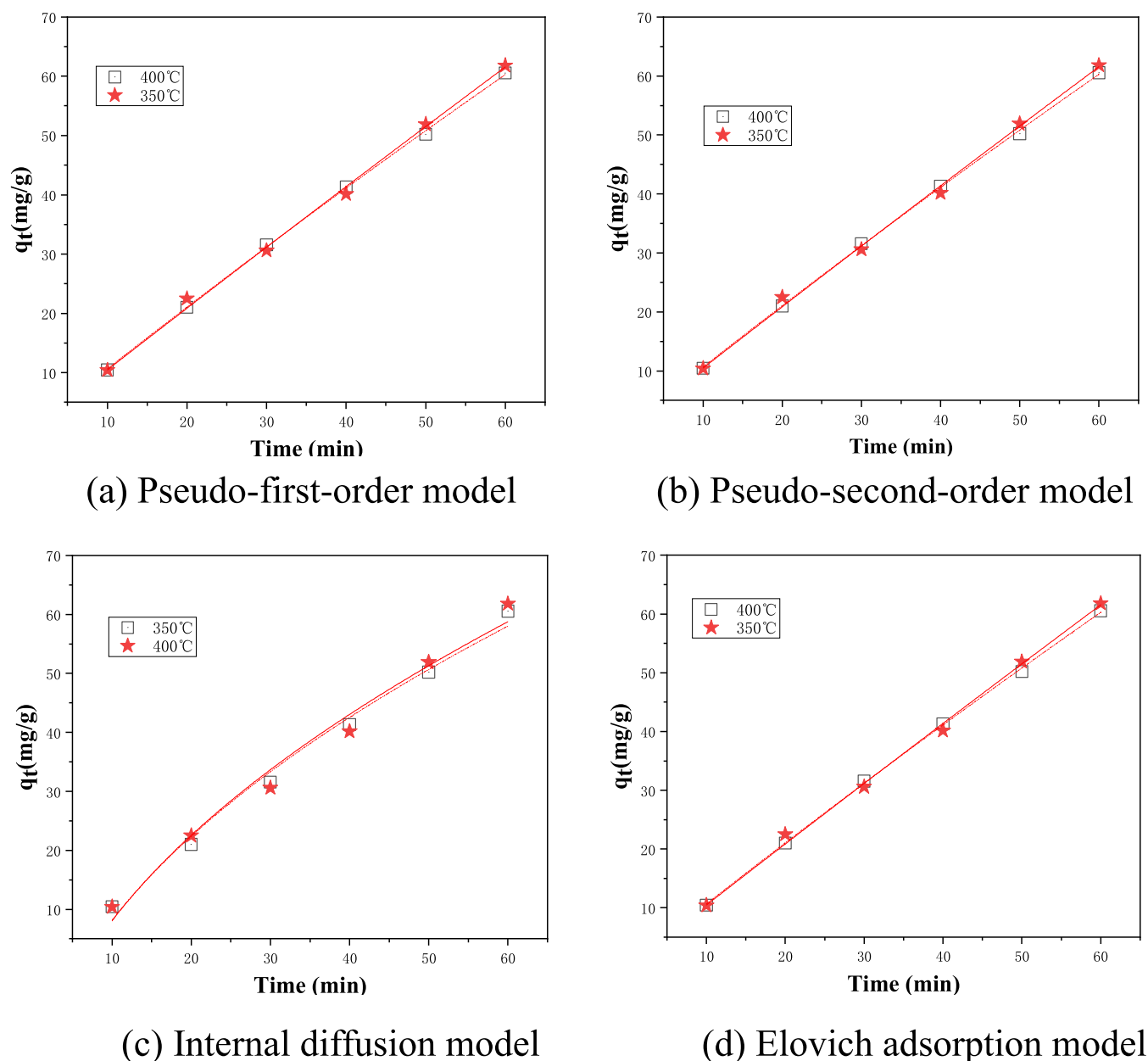
Figure 17. Fitting curve of SO_3 adsorption by FA1-1.5 NaOH adsorbent.

SO_3 in the flue gas of coal-fired power plant mainly comes from the combustion process and the SCR catalytic process. Under the influence of many factors, no more than 2% of SO_2 produced by combustion is oxidized to SO_3. In addition, about 1−2% of SO_2 is oxidized to SO_3 under the action of high temperature and catalyst during the SCR catalysis process. The concentration of SO_2 in the flue gas is much higher than that of SO_3. Most of the injected adsorbents would also react with SO_2, leading to the rapid consumption of fresh adsorbents. Pang et al.[55] suggested to screen the adsorbents with high selectivity toward SO_3, providing a reference for the selection of modification agent for raw fly ash. He et al.[18] also found that the increase in SO_2 concentration would weaken the SO_3 adsorption and decrease the SO_3 selectivity, they pointed out that the strong competitive reactions between SO_3 and SO_2 would reduce the effective utilization of SO_3 adsorbents, which needs to be considered during the industrial application. Meanwhile, there is little research on the competitive

adsorption between SO_2 and SO_3, especially for fly ash-based adsorbents. Meanwhile, as the composition of fly ash is relatively complex, the competitive reactions between SO_2 and SO_3 for modified fly ash adsorbents are very complex, which still need further experimental and theoretical investigations.

3.5. Adsorption Kinetics Analysis. The adsorption kinetics of SO_3 by the modified fly ash adsorbent was carried out with four different adsorption kinetics models to explore the underlying adsorption removal mechanism of SO_3 by the modified fly ash adsorbent. In this section, modified fly ash samples prepared by the best modification methods were used to carry out experimental investigation of the change in the SO_3 removal rate with time, which were FA1-1.5 NaOH, FA2-3 NaOH, and FA3-3 NaOH. The relationship between SO_3 accumulated adsorption amount and adsorption time within 60 min (interval of 10 min) was obtained. The particle size of modified fly ash was 0.065−0.074 mm, the concentration of SO_3 was 50 μL/L, the water vapor content was 10%, and N_2

(a) Pseudo-first-order model

(b) Pseudo-second-order model

(c) Internal diffusion model

(d) Elovich adsorption model
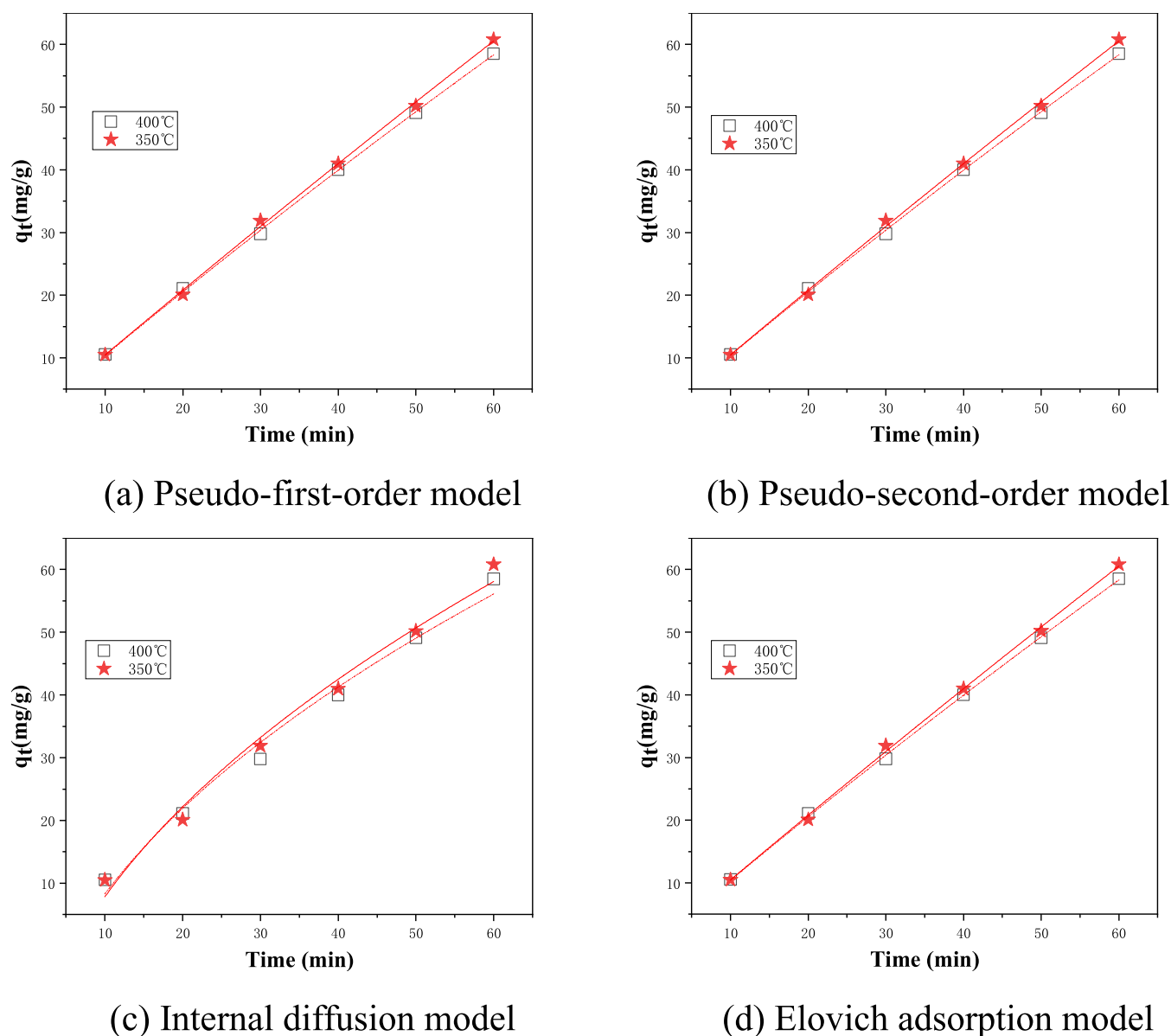
Figure 18. Fitting curve of SO_3 adsorption by the FA2-3 NaOH adsorbent.

was used as the balance gas. The experimental results were analyzed using four adsorption kinetic models (pseudo-first-order kinetic model, pseudo-second-order kinetic model, internal diffusion model, and Elovich adsorption model). The error between the fitting result and the experimental data is represented by correlation coefficient R^2. The larger the R^2 value, the better the model matches the adsorption process.

3.5.1. Pseudo-First-Order Kinetic Model.[56] The pseudo-first-order kinetic model is a new model obtained by modifying the ideal kinetic model, which is mainly used to describe the process of external mass transfer in the adsorption process. The integral expression formula for the adsorption rate is as follows.

$$q_t = q_e(1 - e^{-tk_1}) \tag{2}$$

where q_t is the amount of SO_3 adsorbed per unit mass adsorbent, mg/g, q_e is the adsorption capacity of SO_3 at equilibrium, mg/g, and k_1 is the adsorption rate constant of the pseudo-first-order equation.

3.5.2. Pseudo-Second-Order Kinetic Model.[57] The quasi-second-order kinetic model shows a quadratic relationship between the reaction rate and the reactant concentration in the reaction process, which is mainly used to describe the chemical adsorption, and its integral expression formula for the adsorption rate is as follows.

$$q_t = \frac{q_e^2 k_2 t}{1 + q_e k_2 t} \tag{3}$$

where k_2 is the adsorption rate constant of the pseudo-second-order equation.

3.5.3. Internal Diffusion Model.[58] The internal diffusion model is the one in which the reaction rate is controlled by internal pore diffusion, and its integral expression for the adsorption rate is as follows.

$$q_t = k_3 t^{0.5} + C \tag{4}$$

(a) Pseudo-first-order model

(b) Pseudo-second-order model

(c) Internal diffusion model

(d) Elovich adsorption model
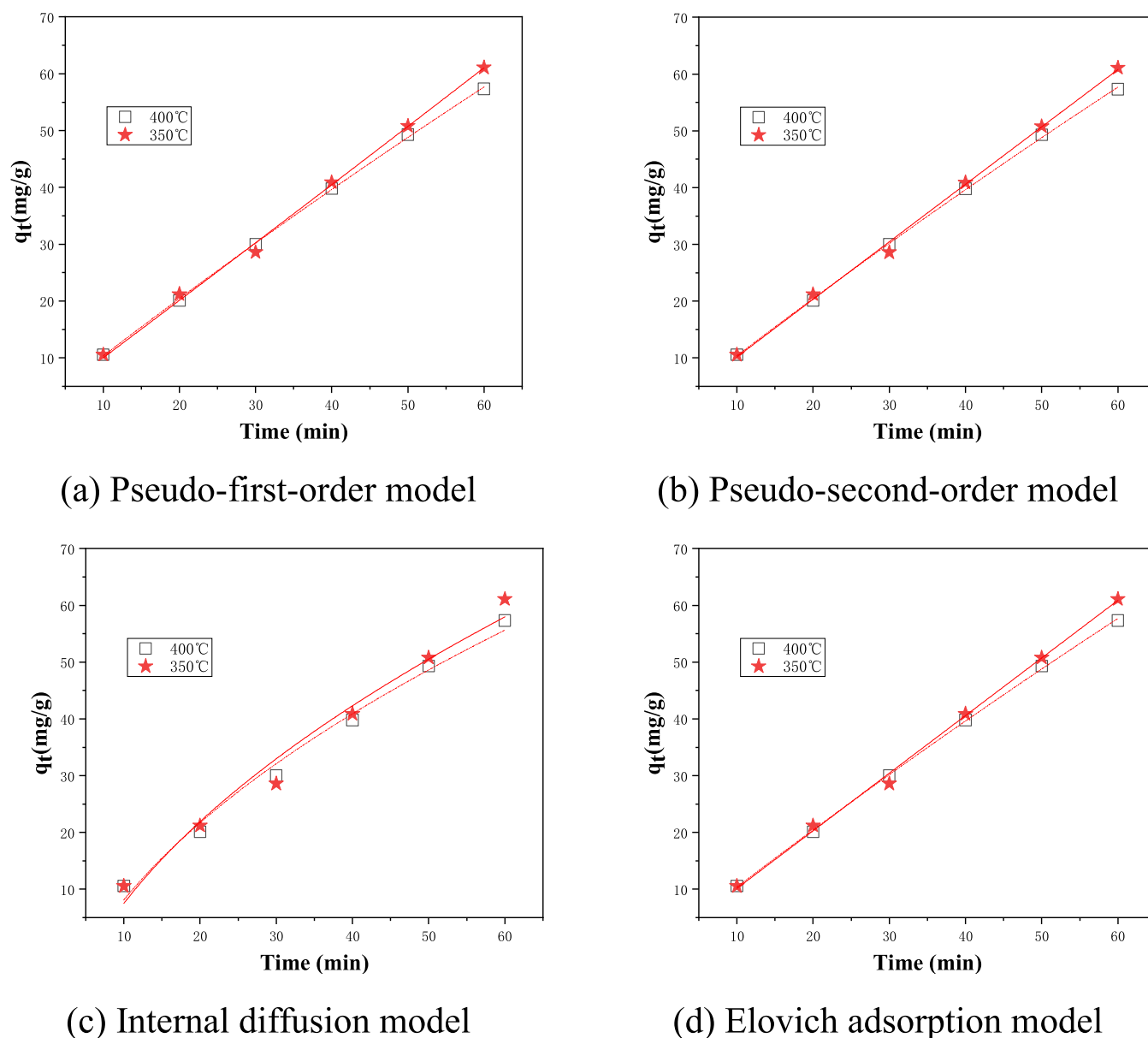
Figure 19. Fitting curve of SO$_3$ adsorption by the FA3-3 NaOH adsorbent.

Table 4. Kinetic Data and Correlation Coefficient R^2 Obtained from Different Models for FA1-1.5 NaOH

model	T (°C)	q_e (mg/g)	k_1	R^2	model	T (°C)	q_e (mg/g)	k_2	R^2
Pseudo-first-order	400	454.26	0.0024	0.99954	Pseudo-second-order	400	878.45	1.37×10^{-6}	0.99963
	350	1271.16	0.00083	0.99628		350	2497.12	1.69×10^{-7}	0.99672
model	T °C	C	k_3	R^2	model	T °C	a (mg/(g·min))	b (g/mg)	R^2
internal diffusion	400	−26.28	10.88	0.98653	Elovich	400	1.08	0.0024	0.99954
	350	−26.91	11.06	0.97716		350	1.05	0.00082	0.99672

where C is a constant and k_3 is the adsorption rate constant of the internal diffusion model.

3.5.4. Elovich Adsorption Model.[59] The Elovich adsorption model is widely used in the chemisorption kinetics of pollutants on the surface of solid sorbents, and its integral expression for adsorption rate is as follows.

$$q_t = \frac{\ln(t + t_0)}{b} - \frac{\ln t_0}{b} \qquad (5)$$

where $t_0 = 1/(ab)$, a is the initial adsorption rate, mg/(g·min) and b is a constant related to surface coverage and activation energy, g/mg.

Figures 17−19 show the fitting curves of experimental data and the adsorption model for modified fly ash adsorbents at 350 and 400 °C, respectively. The pseudo-first-order kinetic model, pseudo-second-order kinetic model, and Elovich adsorption model have a high fitting degree, while the internal diffusion model has a poor fitting degree. This indicates that internal diffusion is not the main mechanism in the removal

Table 5. Kinetic Data and Correlation Coefficient R^2 Obtained from Different Models for FA2-3 NaOH

model	T (°C)	q_e (mg/g)	k_1	R^2	model	T (°C)	q_e (mg/g)	k_2	R^2
Pseudo-first-order	400	382.98	0.0027	0.99943	Pseudo-second-order	400	734.71	1.9×10^{-6}	0.99943
	350	687.02	0.0015	0.99871		350	1344.69	5.8×10^{-7}	0.99892
model	T (°C)	C	k_3	R^2	model	T (°C)	a (mg/(g·min))	b (g/mg)	R^2
internal diffusion	400	−24.72	10.43	0.98415	Elovich	400	1.06	0.0028	0.99943
	350	−26.86	10.96	0.98364		350	1.06	0.00015	0.99875

Table 6. Kinetic Data and Correlation Coefficient R^2 Obtained from Different Models for FA3-3 NaOH

model	T (°C)	q_e (mg/g)	k_1	R^2	model	T (°C)	q_e (mg/g)	k_2	R^2
Pseudo-first-order	400	336.49	0.0031	0.99954	Pseudo-second-order	400	646.74	2.5×10^{-6}	0.99953
	350	3733.32	0.0018	0.99692		350	1212.68	7.1×10^{-7}	0.99679
model	T (°C)	C	k_3	R^2	model	T (°C)	a (mg/(g·min))	b (g/mg)	R^2
internal diffusion	400	−24.64	10.36	0.98603	Elovich	400	1.06	0.0032	0.99962
	350	−27.32	11.01	0.97139		350	1.01	0.0010	0.99684

process of SO_3 by modified fly ash sorbents. The adsorption of SO_3 with modified fly ash adsorbents is significantly dependent on the external mass transfer and chemical adsorption process.

Tables 4−6 list the kinetic data and correlation coefficients R^2. For pseudo-first-order kinetic model and pseudo-second-order kinetic model, the adsorption capacity of SO_3 at equilibrium (q_e) for the three modified fly ash sorbents at 350 °C is larger than that at 400 °C; however, the adsorption rate constants (k_1) at 350 °C are smaller than those at 400 °C, and the correlation coefficient R^2 is larger than 0.99, indicating that the external mass transfer described by the pseudo-first-order model and the chemisorption described by the pseudo-second-order model are the main steps affecting the adsorption efficiency of the modified fly ash sorbent.[60] For internal diffusion model, the adsorption rate constants (k_3) at 350 °C are larger than those at 400 °C, and the correlation coefficient R^2 was larger than 0.9. Compared with the first two kinetic models, the correlation coefficient R^2 was a little smaller, from which it may be inferred that internal diffusion is not the most critical adsorption mechanism in the process of SO_3 adsorption. For the Elovich adsorption model, the correlation coefficient R^2 was larger than 0.99, indicating that adsorption of SO_3 by the modified fly ash adsorbents conforms to the principle of chemical adsorption kinetics on solid adsorbents. The initial adsorption rate (a) obtained by the Elovich adsorption model was very close to the initial adsorption rate ($k_2 q_e^2$) obtained by the Pseudo-second order kinetic equation, which indicates the reliability of the fitting results.[61] It also shows that the chemical adsorption process is the main critical process of SO_3 adsorption by modified fly ash adsorbents.

4. CONCLUSIONS

In this paper, the adsorption performance of SO_3 with modified fly ash adsorbents was investigated using a fixed-bed adsorption experimental system within the temperature range of 250−450 °C. Combined with adsorbent characterization analysis, the adsorption removal mechanism of SO_3 by modified fly ash adsorbents was discussed with different adsorption kinetics models. The results are summarized as follows.

(1) The SO_3 adsorption efficiency of the fly ash samples increases after modification. The fly ash samples modified with NaOH show the greatest adsorption ability of SO_3, while fly ash samples modified with NH_4Br have the poorest SO_3 adsorption ability. The

best adsorption performance of fly ash was achieved when 1.5 mol/L NaOH solution was used, with the highest SO_3 adsorption efficiency of up to 98.3%.

(2) When the modified fly ash adsorbent particle size is in the range of 0.065−0.154 mm, the SO_3 adsorption capacity varies between 56.5 and 60.5 mg/g, and the SO_3 adsorption efficiency is in the range of 91.4−95.5%. The modified fly ash adsorbent particle size has little influence on the SO_3 adsorption efficiency. As the reaction temperature increases from 250 to 450 °C, the SO_3 adsorption efficiency first increases and then decreases, with an optimal reaction temperature of 350 °C.

(3) As the SO_3 concentration increases from 10 to 100 μL/L, the SO_3 adsorption capacity and efficiency decrease. When the water vapor content is in the range of 6−12%, it has little influence on the SO_3 adsorption efficiency. There is no competitive adsorption between SO_3 and NO, however, increasing SO_2 concentration decreases the SO_3 adsorption efficiency of the modified fly ash adsorbents.

(4) The adsorption kinetic data show that external mass transfer and chemical adsorption are the main critical mechanisms affecting the adsorption efficiency of the modified fly ash adsorbent in the SO_3 removal process compared to internal diffusion.

■ AUTHOR INFORMATION

Corresponding Author

    Guiling Xu − *Jiangsu Provincial Key Laboratory of Materials Cycling and Pollution Control, School of Energy and Mechanical Engineering, Nanjing Normal University, Nanjing 210023, China;* ⓞ orcid.org/0000-0001-5995-6398; Phone: (+86)25 85481124; Email: xuguiling@njnu.edu.cn

Authors

    Feihan Chen − *Jiangsu Provincial Key Laboratory of Materials Cycling and Pollution Control, School of Energy and Mechanical Engineering, Nanjing Normal University, Nanjing 210023, China*

    Yangjie Qian − *Jiangsu Provincial Key Laboratory of Materials Cycling and Pollution Control, School of Energy and Mechanical Engineering, Nanjing Normal University, Nanjing 210023, China*

Ping Lu − *Jiangsu Provincial Key Laboratory of Materials Cycling and Pollution Control, School of Energy and Mechanical Engineering, Nanjing Normal University, Nanjing 210023, China*

Miaomin Hong − *Jiangsu Provincial Key Laboratory of Materials Cycling and Pollution Control, School of Energy and Mechanical Engineering, Nanjing Normal University, Nanjing 210023, China*

Qi Zhang − *Jiangsu Provincial Key Laboratory of Materials Cycling and Pollution Control, School of Energy and Mechanical Engineering, Nanjing Normal University, Nanjing 210023, China*

Qiang Zhou − *Jiangsu Provincial Key Laboratory of Materials Cycling and Pollution Control, School of Energy and Mechanical Engineering, Nanjing Normal University, Nanjing 210023, China;* ⊙ orcid.org/0000-0002-5744-2761

Complete contact information is available at:
https://pubs.acs.org/10.1021/acsomega.2c07476

Notes
The authors declare no competing financial interest.

■ REFERENCES

(1) Zhang, Y.; Zheng, C.; Liu, S.; Qu, R.; Yang, Y.; Zhao, H.; Yang, Z.; Zhu, Y.; Gao, X. An investigation of SO_3 control routes in ultra-low emission coal-fired power plants. *Aerosol Air Qual. Res.* **2019**, *9*, 2908−2916.

(2) Zhou, X.; Tang, W.; He, M.; Xiao, X.; Wang, T.; Cheng, S.; Zhang, L. Combined removal of SO3 and HCl by modified Ca(OH)2 from coal-fired flue gas. *Sci. Total Environ.* **2023**, *857*, No. 159466.

(3) Shen, J.; Zheng, C.; Xu, L.; Zhang, Y.; Zhang, Y.; Liu, S.; Gao, X. Atmospheric emission inventory of SO3 from coal-fired power plants in China in the period 2009−2014. *Atmos. Environ.* **2019**, *197*, 14−21.

(4) Liu, L.; Shao, G.; Gong, P.; Wu, Z.; Chu, J.; Hu, Y.; Wang, J.; Wang, S.; Zheng, C.; Gao, X.; et al. Density functional theory studies on ortho-position adsorption of SO_3 at step sites of a CaO surface with SO_2 and CO_2. *Fuel* **2022**, *310*, No. 122174.

(5) Han, Y.; Zhu, Y. Study on the effect of supercritical CFB boiler air preheater and flue gas treatment facilities on sulfur trioxide emission characteristics. *Energy Rep.* **2022**, *8*, 926−939.

(6) Ren, Y.; Wu, Q.; Wen, M.; Li, G.; Xu, L.; Ding, X.; Li, Z.; Tang, Y.; Wang, Y.; Li, Q.; Wang, S. Sulfur trioxide emissions from coal-fired power plants in China and implications on future control. *Fuel* **2020**, *261*, No. 116438.

(7) Dai, G.; Ma, W.; Zhang, J.; Zheng, Y.; Wang, X.; You, H.; Tan, H.; ur Rahman, Z. Experimental and density functional study of sulfur trioxide formation catalyzed by hematite in pressure oxy-combustion. *Fuel* **2022**, *323*, No. 124433.

(8) Qing, M.; Su, S.; Wang, L.; Liu, L.; Xu, K.; He, L.; Jun, X.; Hu, S.; Wang, Y.; Xiang, J. Getting insight into the oxidation of SO_2 to SO_3 over V_2O_5-WO_3/TiO_2 catalysts: reaction mechanism and effects of NO and NH_3. *Chem. Eng. J.* **2019**, *361*, 1215−1224.

(9) Xiang, B.; Zhang, M.; Yang, H.; Lu, J. Prediction of acid dew point in flue gas of boilers burning fossil fuels. *Energy Fuels* **2016**, *30*, 3365−3373.

(10) Zheng, C.; Wang, Y.; Liu, Y.; Yang, Z.; Qu, R.; Ye, D.; Liang, C.; Liu, S.; Gao, X. Formation, transformation, measurement, and control of SO_3 in coal-fired power plants. *Fuel* **2019**, *241*, 327−346.

(11) Zheng, C.; Hong, Y.; Xu, Z.; Li, C.; Wang, L.; Yang, Z.; Zhang, Y.; Gao, X. Experimental study on removal characteristics of SO_3 by wet flue gas desulfurization absorber. *Energy Fuels* **2018**, *32*, 6031−6038.

(12) Pei, T.; Ma, S.; Zhao, G.; Wang, P.; Song, G.; Mi, C.; Wang, F. Study on the Removal Characteristics of SO_3 Acid Mist during the Condensation of Wet Flue Gas. *Ind. Eng. Chem. Res.* **2022**, *61*, 3729−3741.

(13) He, K.; Song, Q.; Yan, Z.; Zheng, N.; Yao, Q. Study on competitive absorption of SO_3 and SO_2 by calcium hydroxide. *Fuel* **2019**, *242*, 355−361.

(14) Wang, H.; Chen, D.; Li, Z.; Zhang, D.; Cai, N.; Yang, J.; Wei, G. SO_3 removal from flue gas with Ca(OH)2 in entrained flow reactors. *Energy Fuels* **2018**, *32*, 5364−5373.

(15) Zheng, C.; Luo, C.; Liu, Y.; Wang, Y.; Lu, Y.; Qu, R.; Zhang, Y.; Gao, X. Experimental study on the removal of SO_3 from coal-fired flue gas by alkaline sorbent. *Fuel* **2020**, *259*, No. 116306.

(16) Mathieu, Y.; Tzanis, L.; Soulard, M.; Patarin, J.; Vierling, M.; Molière, M. Adsorption of SO_x by oxide materials: A review. *Fuel Process. Technol.* **2013**, *114*, 81−100.

(17) Xie, D.; Wang, H.; Tao, J.; Chang, D.; You, C. Sulfur trioxide removal performance of alkaline sorbents injection in the temperature range 400−705 degrees C: a pilot-scale study. *J. Chem. Technol. Biotechnol.* **2019**, *94*, 2382−2388.

(18) He, K.; Song, Q.; Yan, Z.; Yao, Q. SO3 Removal from Flue Gas by Using Na2SO3. *Energy Fuels* **2020**, *34*, 7232−7241.

(19) Wang, Z.; Hu, Y.; Cheng, X.; Ma, C. Study of adsorption characteristics of calcium-based sorbents with SO_3. *Energy Procedia* **2018**, *144*, 43−49.

(20) He, K.; Tang, Z.; Song, Q.; Yao, Q. Process analysis of SO_3 removal by Ca(OH)2 particles from flue gas. *Chem. Eng. Sci.* **2022**, *247*, No. 117054.

(21) Steward, F. R.; Karman, D.; Kocaefe, D. A comparison of the reactivity of various metal oxides with SO_3. *Can. J. Chem. Eng.* **1987**, *65*, 342−344.

(22) Thibault, J. D.; Steward, F. R.; Ruthven, D. M. The kinetics of absorption of SO_3 in calcium and magnesium oxides. *Can. J. Chem. Eng.* **1982**, *60*, 796−801.

(23) Galloway, B. D.; Sasmaz, E.; Padak, B. Binding of SO3 to fly ash components: CaO, MgO, Na2O and K2O. *Fuel* **2015**, *145*, 79−83.

(24) Allen, D.; Hayhurst, A. N. Kinetics of the reaction between gaseous sulfur trioxide and solid calcium oxide. *J. Chem. Soc., Faraday Trans.* **1996**, *92*, 1239−1242.

(25) Tang, W.; Zhang, L.; Luo, H. Experimental Study on the Removal of Low-Concentration SO3 by Trona at Medium Temperatures. *Ind. Eng. Chem. Res.* **2021**, *60*, 8947−8956.

(26) Rathnayake, M.; Julnipitawong, P.; Tangtermsirikul, S.; Toochinda, P. Utilization of coal fly ash and bottom ash as solid sorbents for sulfur dioxide reduction from coal fired power plant: Life cycle assessment and applications. *J. Cleaner Prod.* **2018**, *202*, 934−945.

(27) Wang, S.; Wu, H. Environmental-benign utilisation of fly ash as low-cost adsorbents. *J. Hazard. Mater.* **2006**, *136*, 482−501.

(28) Guo, B.; Zhang, J.; Wang, Y.; Qiao, X.; Xiang, J.; Jin, Y. Study on CO_2 adsorption capacity and kinetic mechanism of CO_2 adsorbent prepared from fly ash. *Energy* **2023**, *263*, No. 125764.

(29) Spörl, R.; Walker, J.; Belo, L.; Shah, K.; Stanger, R.; Maier, Jr.; Wall, T.; Scheffknecht, Gn. SO_3 emissions and removal by ash in coal-fired oxy-fuel combustion. *Energy Fuels* **2014**, *28*, 5296−5306.

(30) Romero, C. E.; Vahedi, N.; Yao, Z.; Stenger, H. G. Modeling of SO3 formation and depletion processes in coal-fired boilers. *Fuel* **2020**, *280*, No. 118355.

(31) Rubio, B.; Izquierdo, M. Coal fly ash based carbons for SO_2 removal from flue gases. *Waste Manage.* **2010**, *30*, 1341−1347.

(32) Yang, B.; Ma, S.; Cui, R.; Wang, J.; Sun, S.; Li, S. Novel low-cost simultaneous removal of NO and SO_2 with· OH from decomposition of H_2O_2 catalyzed by alkali-magnetic modified fly ash. *Ind. Eng. Chem. Res.* **2019**, *58*, 5339−5347.

(33) Zhao, J.; Zheng, X.; Fan, B.; Song, K.; Jiang, H. Experimental Study on SO_2 Removal by Manganese-loaded Fly Ash Adsorbents *Proceedings of the CSEE* 2019.

(34) Baldwin, A. C. Heterogeneous reactions of sulfur dioxide with carbonaceous particles. *Int. J. Chem. Kinet.* **1982**, *14*, 269−277.

(35) Wang, S. *Study on the Adsorption of Ammonium Bromide Modified Fly Ash to Sulfur Trioxide*; North China Electric Power University, 2018.

(36) Purbasari, A.; Ariyanti, D.; Sumardiono, S.; Shofa, M. A.; Manullang, R. P. Comparison of Alkali Modified Fly Ash and Alkali Activated Fly Ash as Zn(II) Ions Adsorbent from Aqueous Solution. *Sci. Sintering* **2022**, *54*, 49−58.

(37) Dindi, A.; Dang Viet, Q.; Nashef, E.; Abu Zahra, M. R. M. *Effect of PEI Impregnation on the CO2 Capture Performance of Activated Fly Ash*, 13th International Conference on Greenhouse Gas Control Technologies (GHGT), Lausanne, Switzerland, Nov 14−18, 2017; Lausanne, Switzerland, 2016; pp 2243−2251.

(38) Gao, X.; Dai, Y.; Zhang, Y.; Zhai, X.; Fu, F. Effective Dye Removal From Waste Water Using A Novel Low-cost NaOH-Modified Fly Ash. *Clays Clay Miner.* **2016**, *64*, 695−705.

(39) Tian, Y. *Study on Modification and Adsorption Properties of Fly Ash*; Anhui University of Science & Technology, 2017.

(40) Li, H.; Chen, Y.; Cao, Y.; Liu, G.; Li, B. Comparative study on the characteristics of ball-milled coal fly ash. *J. Therm. Anal. Calorim.* **2016**, *124*, 839−846.

(41) Liu, J.; Wang, Q. P.; Min, F. F. Modification of fly ash and its adsorption of oily wastewater. *New Chem. Mater.* **2017**, *45*, 243−245.

(42) Zhang, Y.; Mei, D.; Wang, T.; Wang, J.; Gu, Y.; Zhang, Z.; Romero, C. E.; Pan, W.-p. In-situ capture of mercury in coal-fired power plants using high surface energy fly ash. *Environ. Sci. Technol.* **2019**, *53*, 7913−7920.

(43) Luo, Y.; Ma, S.; Liu, C.; Zhao, Z.; Zheng, S.; Wang, X. Effect of particle size and alkali activation on coal fly ash and their role in sintered ceramic tiles. *J. Eur. Ceram. Soc.* **2017**, *37*, 1847−1856.

(44) Jun, W.; Yilin, Y.; Zenghe, L. Removal of Pb²⁺ by waste incineration fly ash composite. *Sci. Technol. Chem. Ind.* **2019**, *27*, 50−55.

(45) Xiaolu, C.; Qinxin, Z. Experimental Research on SO₃ Removal. *J. Chin. Soc. Power Eng.* **2014**, *34*, 966−971.

(46) Xu huang, R. H.; Xianrong, Zheng. Experimental study on the removal of SO₂ from simulated flue gas by calcium-based hydrated fly ash adsorbent. *Sci. Technol. Eng.* **2017**, *17*, 108−114.

(47) Yu, X.-R.; Liu, F.; Wang, Z.-Y.; Chen, Y. Auger parameters for sulfur-containing compounds using a mixed aluminum-silver excitation source. *J. Electron Spectrosc. Relat. Phenom.* **1990**, *50*, 159−166.

(48) Sun, Q.; Cui, P.; Wu, S.; Liu, C.; Fan, T.; Alves, M. E.; Cheng, H.; Huang, M.; Zhou, D.; Wang, Y. Role of reduced sulfur in the transformation of Cd (II) immobilized by δ-MnO₂. *Environ. Sci. Technol.* **2020**, *54*, 14955−14963.

(49) Di, G.; Zhou, Q.; Tao, X.; Shang, Y.; Song, T.; Lu, P.; Xu, G. Preparation of sulfur-doped mesoporous carbon and its mercury removal. *Huagong Jinzhan/Chem. Ind. Eng. Prog.* **2022**, *41*, 2761−2769.

(50) Kim, C.; Yeom, M. S.; Kim, E. Hydrogen bond dynamics in liquid water: Ab initio molecular dynamics simulation. *Korean J. Chem. Eng.* **2016**, *33*, 255−259.

(51) Zapata, P. A.; Faria, J.; Pilar Ruiz, M.; Resasco, D. E. Condensation/hydrogenation of biomass-derived oxygenates in water/oil emulsions stabilized by nanohybrid catalysts. *Top. Catal.* **2012**, *55*, 38−52.

(52) Ai, X.; Deng, F.; Dong, J.; Chen, L.; Ye, C. Stability of layered sodium disilicate during hydration process as studied by multinuclear solid state NMR spectroscopy. *J. Phys. Chem. B* **2002**, *106*, 9237−9244.

(53) Kocaefe, D.; Karman, D.; Steward, F. Comparison of the sulfation rates of calcium, magnesium and zinc oxides with SO₂ and SO₃. *Can. J. Chem. Eng.* **1985**, *63*, 971−977.

(54) Zhong, L.; Zhang, Y.; Liu, Z.; Sui, Z.; Cao, Y.; Pan, W.-P. Study of mercury adsorption by selected Chinese coal fly ashes. *J. Therm. Anal. Calorim.* **2014**, *116*, 1197−1203.

(55) Pang, X.; Liu, W.; Xu, H.; Hong, Q.; Cui, P.; Huang, W.; Qu, Z.; Yan, N. Selective uptake of gaseous sulfur trioxide and mercury in ZnO-CuS composite at elevated temperatures from SO2-rich flue gas. *Chem. Eng. J.* **2022**, *427*, No. 132035.

(56) Hashem, A.; Sanousy, M.; Mohamed, L. A.; Okoye, P. U.; Hameed, B. Natural and low-cost P. turgidum for efficient adsorption of Hg (II) ions from contaminated solution: isotherms and kinetics studies. *J. Polym. Environ.* **2021**, *29*, 304−312.

(57) Wang, F.; Tan, S.; Cao, Y.; Wang, D.; Wu, J.; Luo, F.; Liu, Q.; Xie, X.; Li, S.; Zhou, M. Experimental Study on the Influence of Surface Characteristics of Activated Carbon on Mercury Removal in Flue Gas. *Energy Fuels* **2020**, *34*, 6168−6177.

(58) Liu, Z.; Adewuyi, Y. G.; Shi, S.; Chen, H.; Li, Y.; Liu, D.; Liu, Y. Removal of gaseous Hg0 using novel seaweed biomass-based activated carbon. *Chem. Eng. J.* **2019**, *366*, 41−49.

(59) Qiang, Z.; Yufeng, D.; Yongqiu, M.; Chun, Z. Kinetics and mechanism of activated carbon adsorption for mercury removal. *Proc. CSEE* **2013**, *33*, 10−17.

(60) Fu, S.-m.; Chen, M.-l.; Lu, P. Experimental study on mercury adsorption capability on modified Ca-BASED sorbents. *Environmental Engineering*, 2018.

(61) Zhou, Q.; Di, G.; Song, T.; Lu, P.; Xu, G. Template synthesis of sulfur-doped mesoporous carbon for efficiently removing gas-phase elemental mercury from flue gas. *Fuel* **2022**, *321*, No. 124112.